Alex

UCRL 8753

UNIVERSITY OF CALIFORNIA

Ernest O. Lawrence

Radiation Laboratory

SCATTERING OF K^+ MESONS OFF PROTONS

DISCLAIMER

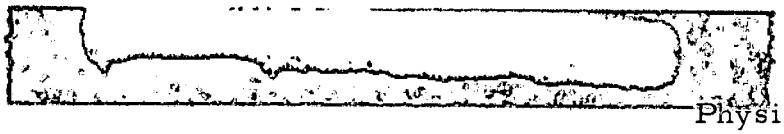

UCRL-8753
Physics and Mathematics

UNIVERSITY OF CALIFORNIA

Lawrence Radiation Laboratory
Berkeley, California

Contract No. W-7405-eng-48

SCATTERING OF K^+ MESONS OFF PROTONS

Thaddeus Francis Kycia
(Thesis)

May 14, 1959

Printed for the U. S. Atomic Energy Commission

Printed in USA. Price $2.25. Available from the
Office of Technical Services
U. S. Department of Commerce
Washington 25, D. C.

Contents

ABSTRACT

The total K^+-p cross section was measured at the three K^+-meson energies 175 ± 25, 225 ± 25, and 275 ± 25 Mev and the differential scattering cross section was measured at 225 Mev. The K^+-p nuclear force was shown to be repulsive from the observed constructive interference with Coulomb scattering. The differential cross section was otherwise isotropic and could arise from either pure S-wave or pure P-wave scattering.

Subtracted dispersion relations were applied to these data and the rest of the available K proton scattering data. The statistical errors on the data were found to be too large to determine the K-hyperon relative parity. However, if the $K\Lambda$ and $K\Sigma$ relative parities are assumed to be the same, then if the coupling were scalar, the coupling constant $g^2/4\pi$ would be less than 0.6; if pseudoscalar, less than 10.

I. INTRODUCTION

Information on the scattering of K^+ mesons on protons is of the greatest importance in that it may allow us to determine the nature of the K-meson-nucleon forces. Data at low energies have come mostly from the rare scattering of K^+ mesons on hydrogen nuclei in emulsion. A compilation of the world total of 75 events was reported at the 1958 High Energy Physics Conference at Cern.[1] The angular distributions in the three energy intervals 20 to 100 Mev, 100 to 200 Mev, and 200 to 300 Mev, due to the large uncertainties were not inconsistent with isotropy.

From a more recent compilation of data,[2] total cross sections have been obtained as shown in Table I.

Table I

Results from emulsion events

Energy (Mev)	Total K^+-p cross sections (mb)
20 - 100	13.5 ± 2.8
100 - 200	14.2 ± 2.6
200 - 300	18.0 ± 3.5

The angular distribution of the events corresponding to the 200-300-Mev energy interval is given in Fig. 1.[2]

The purpose of this experiment was to measure the total K^+-meson-proton cross section at the higher energies--namely, 175 ± 25, 225 ± 25, and 275 ± 25 Mev--as well as to determine the differential-scattering cross

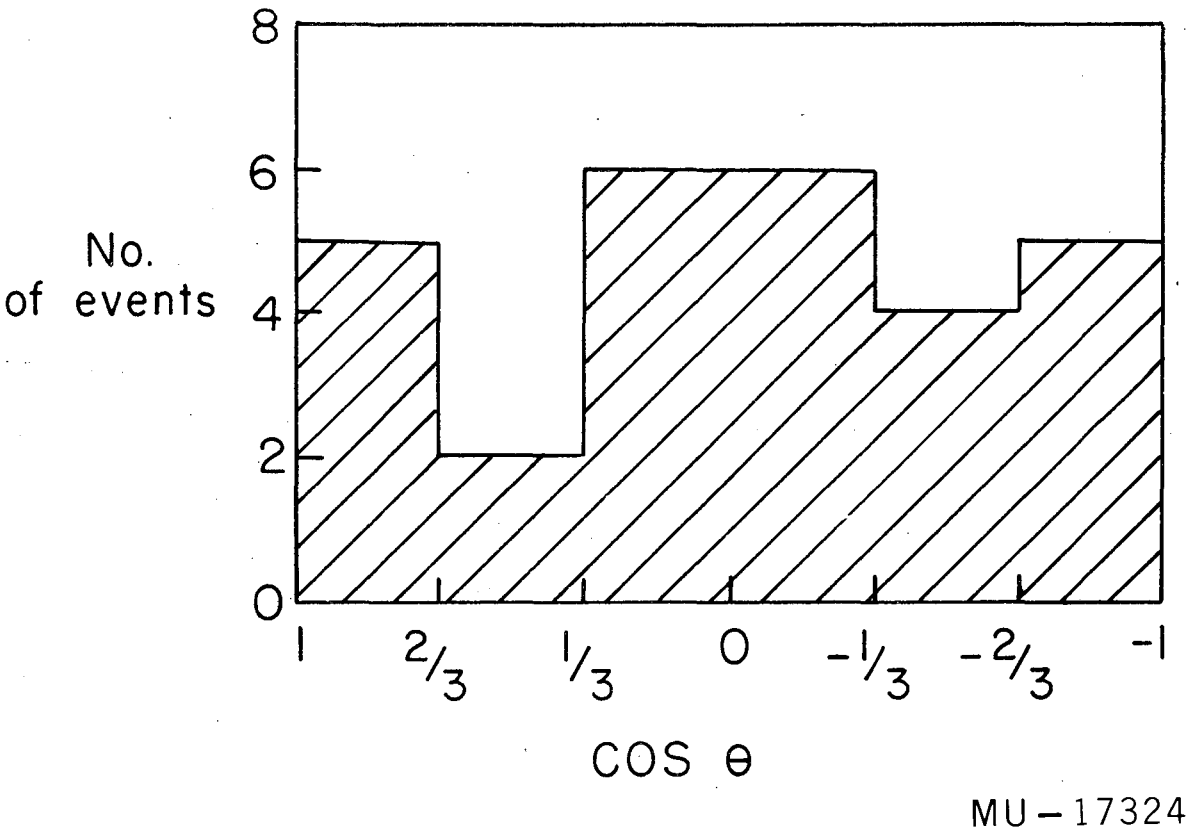

Fig. 1. Angular distribution (c. m.) of K^+ mesons scattering off free protons in emulsion in the energy interval 200 to 300 Mev.

section with small statistical errors at 225 Mev. If the rise in total cross section should be due to a rising P-wave contribution, an asymmetry in the differential-scattering cross section should be seen.

The application of dispersion relations to the determination of the relative K-meson-hyperon parity is discussed.

II. K^+-MESON SELECTION

A. The K^+ Beam

The K^+ beam was set up for three K^+-meson energies; namely, 175±25 Mev, 225±25 Mev, and 275±25 Mev. Figure 2 shows the experimental arrangement of the beam. The tantalum production target was situated in the west straight section of the Bevatron. It was 5 cm long in the direction of the proton beam and presented a cross section of 0.63x4.3 cm in the K^+-beam direction at 60° to the proton beam.

Both the bending magnets were of the two-lens, strong-focusing type, having a 4-inch aperture. The first magnet momentum-analyzed the accepted particles coming from the production target, and, at the same time, refocused them at the lead slit, which then selected particles of the desired momentum. The beryllium helped to separate in momentum the protons from the K^+ mesons coming down the channel. The second magnet then canceled the divergence of the desired particles and refocused the particles with the K^+-meson momentum at the defining scintillation counter. The scattering-detection system set the following requirements on the K^+ beam:

1. The angular divergence of the K^+ mesons should be less than ± 2°;
2. They should be focused on an area 1.25 in. in diameter;
3. The energy spread of the K^+ mesons should be no greater than about ± 25 Mev; and

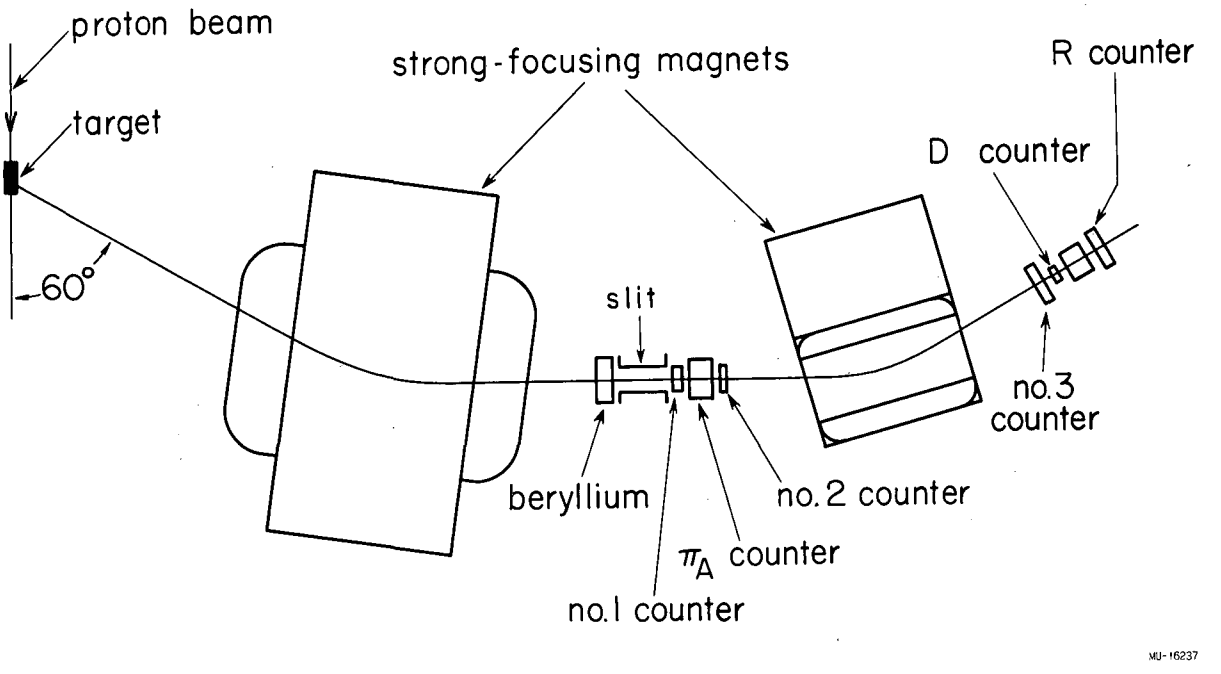

Fig. 2. The K^+-meson beam. The two magnets select K^+ mesons of the desired momentum and focus them behind the D counter. Beryllium was used to separate the K^+ mesons from protons and the various counters were used to identify K^+ mesons in the beam.

4. The number of K^+-mesons per Bevatron pulse should exceed 25.

B. Electronics for the K^+-Meson Identification System

As seen above, the π^+ mesons, K^+ mesons, and protons that are accepted by the lead slit at the first focus are of the same momentum. Because of their mass differences, their velocities are different. Thus the K^+ mesons can be identified by their transit times over the 8-foot length of the counter telescope from counter No. 1 to the D counter. Figure 3 shows a block diagram of the counters and electronics associated with the identification of K^+ mesons. A description of the counters follows.

Scintillation counters Nos. 1, 2, and 3 were $\frac{1}{4}$ in. thick in the beam direction and 3x3 in. in cross section. They were coupled optically to 7264-type RCA photomultiplier tubes by means of Lucite light pipes. Scintillation counters D and R were also $\frac{1}{4}$ in. thick in the beam direction, the former being cylindrical in shape with a 1.25-in. diameter and the latter square in shape with 3-in. sides. Each of these counters was mounted on a 6810A-type RCA photomultiplier tube also using Lucite light pipes. In order to avoid false counts due to Cherenkov radiation in the light pipes of these counters, all the counters were placed in a vertical position with their light pipes below the beam.

The π_B counter is a velocity-threshold Cherenkov counter which identifies π^+ mesons in the beam. Its radiator consists of a clear liquid, Fluorochemical FC-75, manufactured by the Minnesota Mining and Manufacturing Company. The liquid has an index of refraction of 1.276 and is

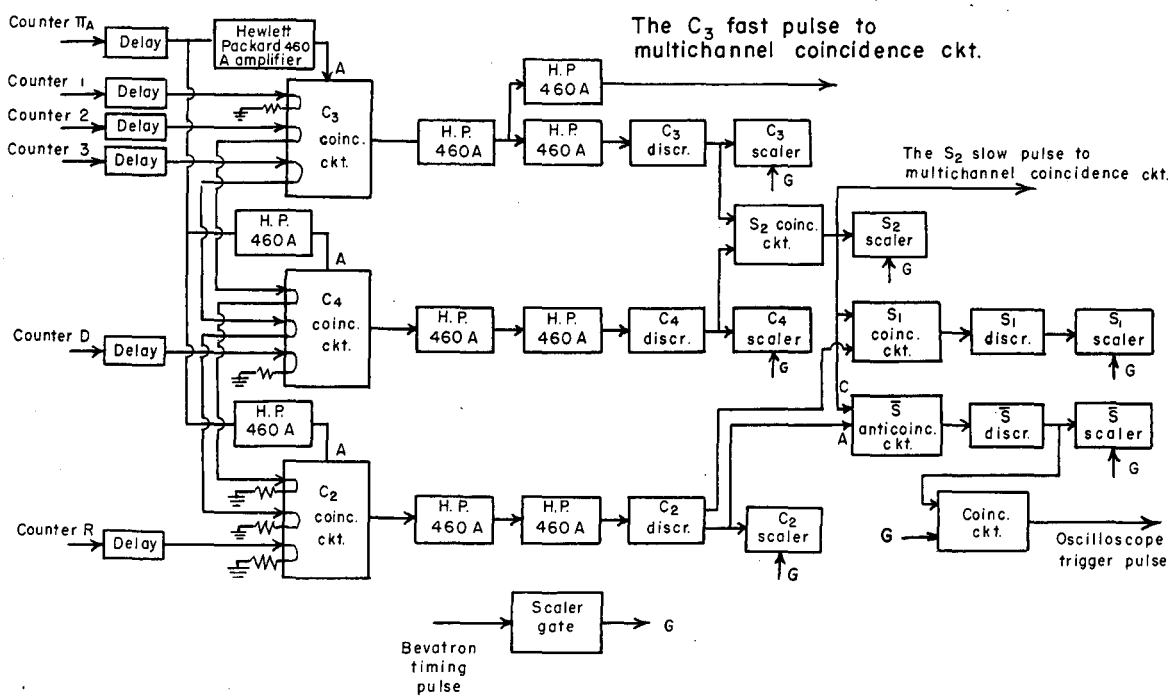

MU-17325

Fig. 3. K^+-meson identification. Coincidences and anticoincidences are taken among counters 1, 2, 3, D, R, and π_A. The S_2 scaler gives the number of incident K^+ mesons; the $\bar{S}$ scaler gives the number of K^+ mesons that are lost between the D and R counters, and the S_1 scaler gives the difference $S_2 - \bar{S}$.

contained in a Lucite cell of 1/16-in. wall thickness, 2.5-in. thickness in the beam direction, and 2.5 x 2.5 in. cross section. The radiation leaving the cell is reflected with a cylindrical aluminum mirror to the photocathode of a 6810-type RCA photomultiplier situated in a vertical position.

The negative anode pulses, after being properly delayed, were connected to the coincidence circuits as shown in Fig. 3. The only exception to this was the π_A pulse, which was divided into three pulses each of which was amplified with a Hewlett-Packard 460A distributed amplifier.

Each of C_2, C_3, and C_4 in Fig. 3 is a threefold millimicrosecond coincidence circuit with an anticoincidence circuit incorporated into it.[3]

Counters 1, 2, and 3 were connected to the inputs of C_3 while counters 2, 3, and D were connected to the inputs of C_4. The reason for having two coincidence circuits and four scintillation counters was simply to improve the time resolution of the system. Coincidence circuits C_3 and C_4 were timed for K^+ mesons, but to improve the rejection ratio for π^+ mesons, the π_A counter was placed in anticoincidence. The purpose of the R counter and C_2 coincidence circuit was for the range-energy measurement of the K^+ mesons, but this is discussed in greater detail later. In Fig. 3 it can be seen that the output pulses of C_3 and C_4 were amplified and then discriminated. The fast discriminator circuit was of the EFP60 type, described in the UCRL drawing #3X1143. The other discriminators in Fig. 3 are the same. The S_2 circuit, which was a

Rossi-type diode coincidence circuit with a 10^{-7}-sec resolution, detected coincidences between the outputs of the C_3 and C_4 discriminators. The outputs of these discriminators as well as the output of the S_2 coincidence circuits were scaled. The S_2 scaler then gave the number of K^+ mesons passing through the counter telescope.

The inputs to the C_2 millimicrosecond coincidence circuit were outputs from counters 3, D, and R. The output of the coincidence circuit was amplified, discriminated against doubles, and scaled. Coincidences with a 10^{-7}-sec resolution were made between the S_2 output and the C_2 discriminator output, and after discrimination against singles, the twofold S_1 coincidences were scaled. Similarly, an anticoincidence requiring that S_2 count and C_2 not count was detected and scaled with the $\bar{S}$ scaler. The $\bar{S}$ scaler then read the number of K^+'s that reached counter D but did not pass through counter R, whereas S_1 was simply $S_2-\bar{S}$, which was equal to the number of K^+ mesons that reached counter D and also counted in R. These counters were used to determine the range distribution of the K^+ mesons in copper inserted between counters D and R. During the data-taking part of the experiment, a liquid hydrogen target was placed between the D counter and a trigger counter, T, which was substituted for the R counter in the electronics. Under the circumstances, whenever a K^+ meson scattered and missed the rear trigger counter T, $\bar{S}$ would count. A pulse from $\bar{S}$ would then trigger the oscilloscope upon whose sweeps the various counter pulses would be displayed. In order to avoid false triggers of the oscilloscope, the $\bar{S}$ oscilloscope trigger was placed in coincidence with a 200-msec. gate, G. This was the same gate

that allowed the scalers to count during the time interval in which the Bevatron proton beam was being spilled onto the target. This scaler gate unit was intitially triggered by a Bevatron timing pulse.

As shown in Figure 3, outputs of C_3 and S_2 coincidence circuits were sent to a multichannel coincidence circuit which took coincidences between the K pulse and the various outputs of the scattering-detection counters. This is discussed in greater detail in the section on the scattering-detection system.

C. Identification of K^+ Mesons

With the combination of counter choice and of fast-coincidence circuits it was possible to distinguish K^+ mesons from π^+ mesons and protons by virtue of their velocity differences. A resolution curve of the K^+-meson identification system at 175 Mev kinetic energy is shown in Figure 4. The delay in counter 1 was varied while the rest of the circuitry was timed for K^+ mesons. Table II lists Δt, the transit-time differences over the 8 ft. of the counter telescope, between K^+ mesons and π^+ mesons and between K^+ mesons and protons at the three energies.

Table II

Transit-time differences

Δt ($m\mu$sec)	Energy (Mev)		
	175±25	225±25	275±25
$\Delta t_{K\pi}$	3.42	2.68	2.13
Δt_{Kp}	6.60	5.5	4.7

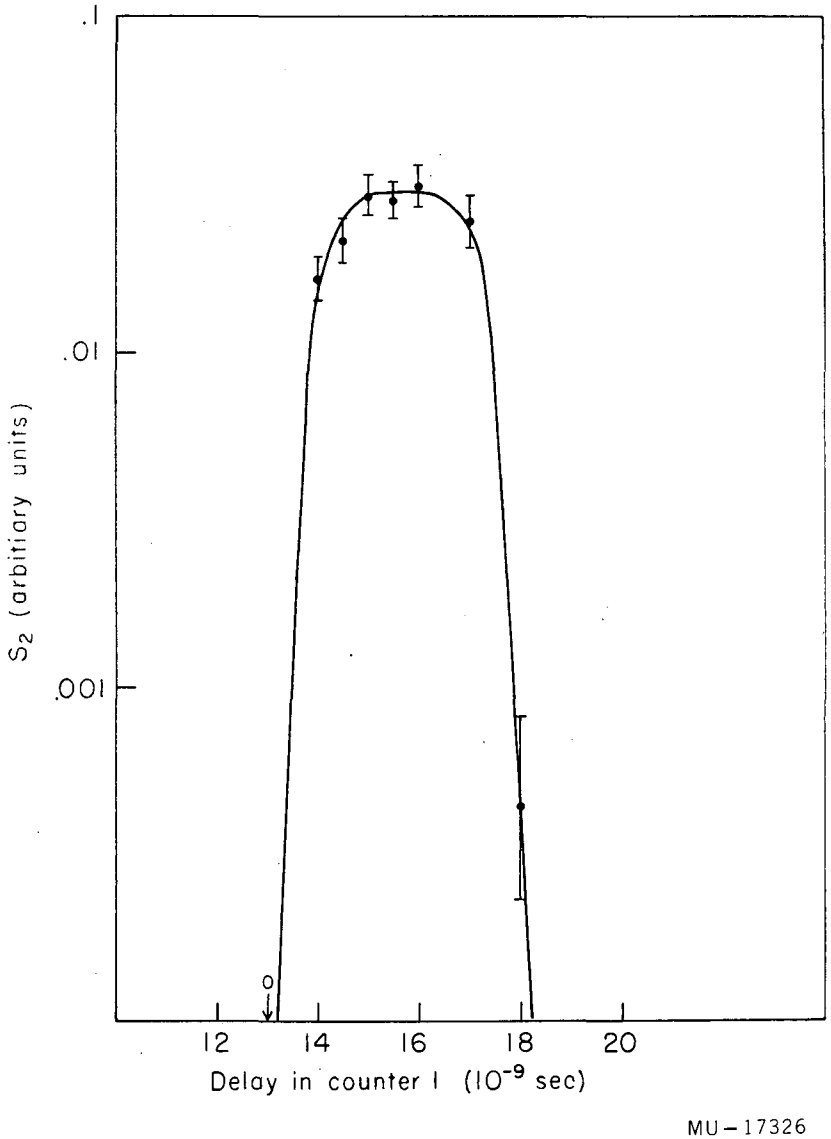

Fig. 4. Resolution curve of the K^+-meson identification system.

By use of this table it is seen in Figure 4 that π^+ mesons would appear at a delay of about 12 mμsec and protons at about 22 mμsec, both outside the resolution curve. The π^+ mesons were rejected mostly by the Cherenkov counter and partly by transit-time difference. Protons, on the other hand, were rejected by transit-time difference. Similar Counter 1 delay curves were obtained at 225 Mev and 275 Mev kinetic energies, but in estimating the π^+-meson contamination, a little more caution was necessary. At either energy the proton peak would fall at delays greater than 20 mμsec, and it can be seen from Figure 4 that they would not give any contribution to S_2 at 15.5 mμsec. The π^+ mesons, however, had their peak at 13.4 m sec. for 275 Mev kinetic energy, and therefore it was necessary to estimate what fraction of the counts at 15.5 mμsec delay was due to π^+ mesons.

When the counter telescope, with the π_A counter turned off, was timed for π^+ mesons, it was found that the ration of π^+ to K^+ was about 100 to 1. The telescope was then timed 2 mμsec off the π^+-meson peak in the direction away from the K^+-meson peak, to make certain that only π^+ were being identified. The π flux was observed for the π_A counter turned off and on. The ratio of the fluxes was 1500 to 1, and this then gave the efficiency of the π_A counter for π^+ mesons. The rejection of π^+ mesons by transit-time difference was better than 10 to 1 when the identification system was timed for K^+ mesons. The result of these two effects was to reduce the π^+-meson contamination of K^+ mesons to less than 0.7%.

The energy distribution of the K^+ mesons was determined by their range in copper. In Figure 5 is shown a range-distribution curve for the K^+ beam at 225±25 Mev kinetic energy. The copper was inserted into the K^+ beam ahead of the R counter. Similar curves were obtained for the 175±25-Mev and 275±25-Mev kinetic energies. It is to be noticed that the range curve has a tail of several percent. It was necessary to show that this tail was not due to π^+ mesons. The probable explanation is that the K^+ mesons that stopped in the copper decayed and sent the charged decay into the R counter.

The half width of the resolution of the S_1 coincidence-circuit combination was about 2.5 mμsec, and the mean life of the K^+ mesons is 12.2 mμsec,[4] so that 18.5% of the K^+ mesons that decayed at rest in the copper would have been timed correctly to count in the range counter. A decay curve was taken on the R counter and the results are plotted on Figure 6. It can be seen that, with 100.2 g of copper in, the counting rate of K^+ mesons does drop off exponentially with a slope corresponding to the mean life of K^+ mesons. Had there been a strong π^+-meson contamination, the K^+-meson counting rate would have dropped noticeably when the delay was changed from 0 to 2 mμsec.

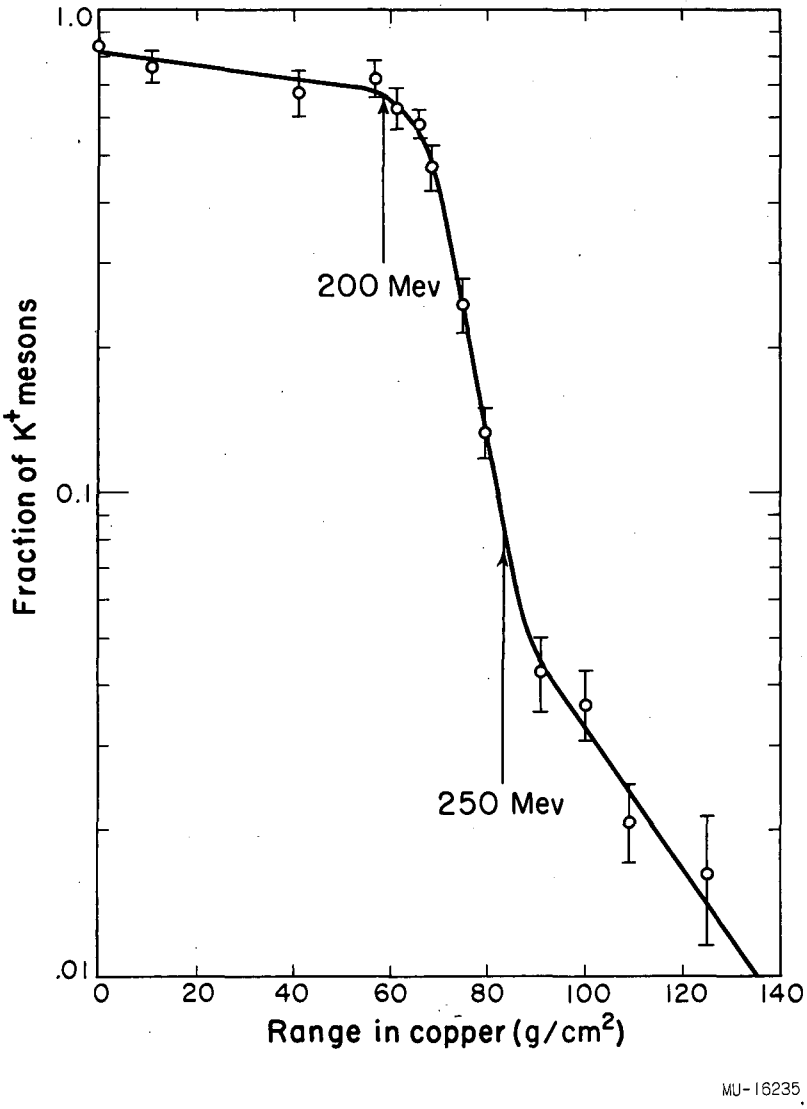

Fig. 5. Range distribution in copper for K^+ mesons with the 225 ± 25 Mev kinetic energy.

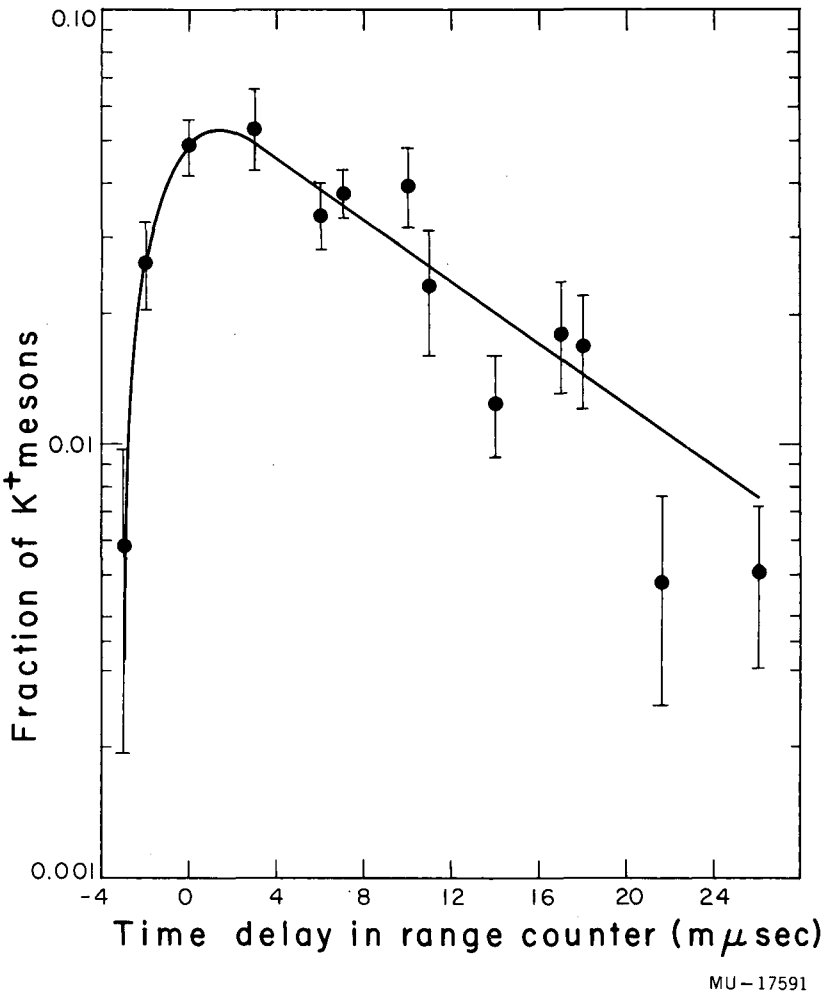

Fig. 6. Counting rate vs. delay in the range counter. The data show that the tail in the range distribution of Fig. 5 is due to K^+ mesons stopping in the copper and sending the decay products into the range counter. The falling off in the counting rate with increase in delay is consistent with a K^+-meson mean life of 1.22×10^{-8} sec.

III SCATTERING-DETECTION SYSTEM

A. Principle

In any kind of scattering experiment one always tries to obtain as many events as possible and as little background as possible in order to arrive at statistically sound cross sections. This was especially the problem with the scattering of K^+ mesons on protons, since the K^+ mesons are somewhat rare, and free protons do not come in high densities. The relationship between all these quantities is summarized as

$$\left.\frac{dN}{d\Omega}\right|_L \Delta\Omega_L = N_p N_K \left.\frac{d\sigma}{d\Omega}\right|_L \Delta\Omega_L \qquad (1)$$

where N_p is the number of protons per square centimeter,

N_K is the number of incident K^+ mesons,

$\left.\frac{d\sigma}{d\Omega}\right|_L$ is the differential K^+-meson-proton cross section in the in the laboratory system,

$\Delta\Omega_L$ is an increment of solid angle,

and $\left.\frac{dN}{d\Omega}\right|_L \Delta\Omega_L$ is the number of K^+ mesons that scattered per unit solid angle into the solid-angle interval $\Delta\Omega_L$.

At the K^+-meson energies used in this experiment identification of a K^+-meson-proton scatter could not have been easily done by detecting a coincidence between the K^+ meson and the recoil proton, because the recoil proton had too low an energy.

Figure 7 shows the kinematic relationship between the center-of-mass-system scattering angle of the K^+ meson and the laboratory-system angles

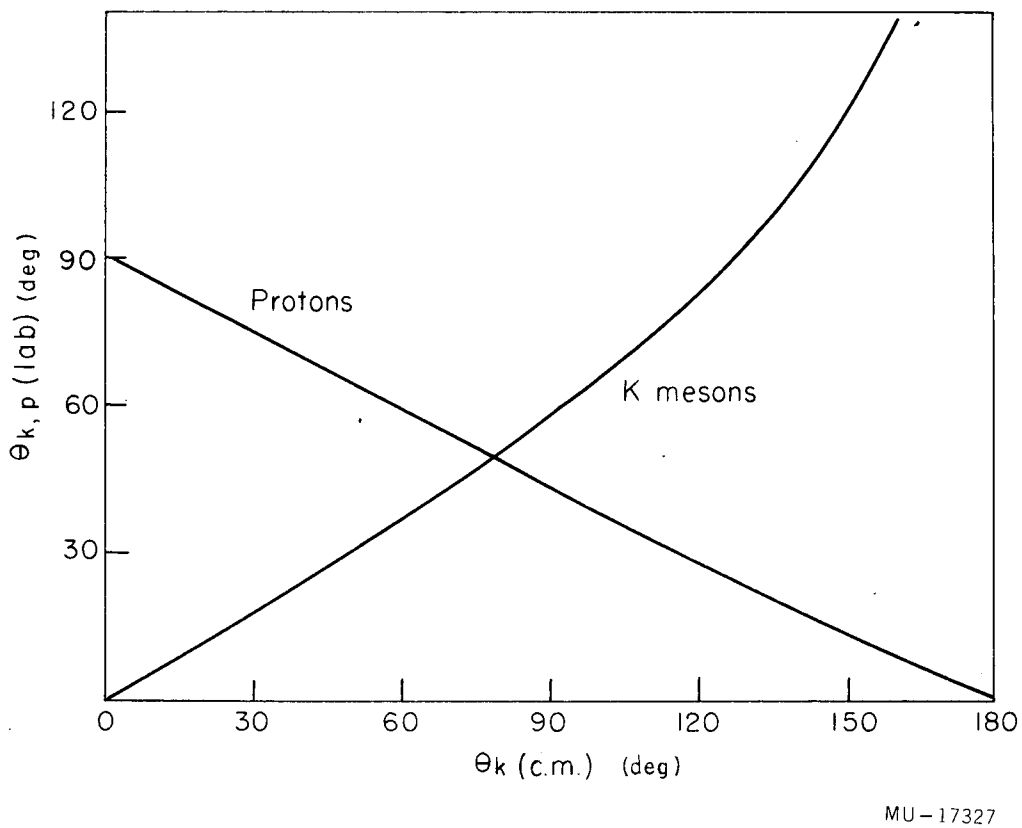

Fig. 7. Relationship between the lab angles of the scattered K^+ meson and recoiling proton and $\theta_{K'}$ the c. m. scattering angle of the K^+ meson.

of both the recoil proton and the scattered K^+ meson. It can be seen that for any elastic scattering only one of the two particles enters a forward cone of half angle 50° (lab). Thus, in order to find the angular distribution of the scattered K^+ mesons, it was sufficient to determine the angle of the forward particle in the cone and then to identify it as being either a K^+ meson or a proton. The inelastic scattering of K^+ mesons giving rise to -meson production is presumed to be small.[5]

B. Target

A liquid hydrogen target assembly was designed for the experiment, but its design is such that it can be easily adapted to various types and sizes of hydrogen vessels for other experiments. Views of the interchangeable target are shown in Figure 8, a drawing of the complete target assembly can be found on UCRL Drawing No. 7A6005B. In Fig. 8, a is the Mylar vessel 6 in. in length, 3 in. in diameter, 0.008 in. in thickness at the ends, and 0.015 in. in thickness at the cylindrical surface. Tube b was connected to the bottom of a 2.5-liter liquid hydrogen reservoir and tube c to the vent through a valve. A liquid nitrogen jacket that surrounded the hydrogen reservoir was in thermal contact with the copper heat shield, d , to reduce heat absorption by the hydrogen. For heat shielding of the ends, thin copper sheets e were used. The entrance window f was made of Mylar, whereas the exit window g was disc-shaped and made of stainless steel. Lucite windows h were situated at each side of the target.

The major boil-off occurred inside the Mylar target itself because

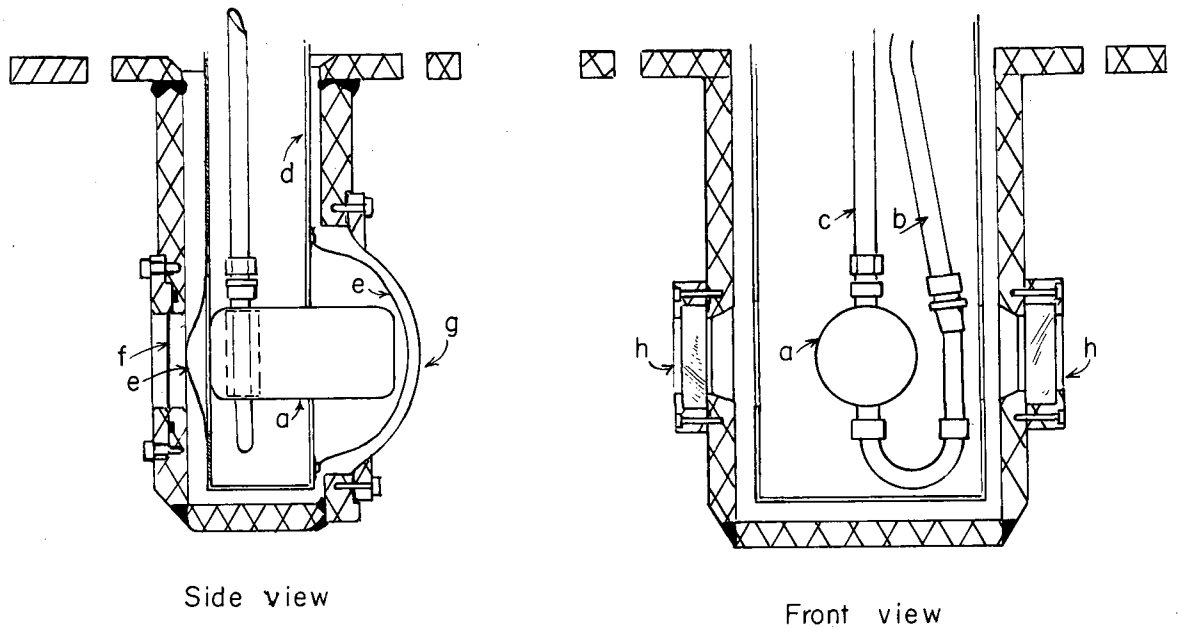

Fig. 8. The liquid hydrogen target; a is the Mylar vessel 6 in. in length, 3 in. in diameter; b is a tube connected to the bottom of a liquid hydrogen reservoir (not shown); c is a tube connected to a vent (not shown); d is a copper heat shield in thermal contact with a nitrogen jacket (not shown); e is a thin copper sheet also used as a heat shield; f is the Mylar entrance window and g the stainless steel exit window; and h is a Lucite window at each side of the target.

of heat absorption through the holes in the heat shield in front of the windows h .

C. Ring Counters

The angle of the particle going forward in a K^+-meson-proton collision was designed with 15 ring counters forming two concentric cones directly behind the target (Figure 9). Efficiencies of these counters at various points on the counter were checked by the following method before the experiment was begun. A Sr^{90}-Y^{90} β-ray source was placed over the counter and a tiny scintillation counter beneath it. When a β ray of sufficient energy passed through the ring counter and penetrated the counter underneath, the latter counter triggered an oscilloscope and the output pulse of the ring counter was displayed on the sweep. A pulse-height distribution was thus obtained. By fitting a Poisson distribution to these data, it was possible to estimate the probability that no pulse would appear at the output and thus the inefficiency of the counter at that point. The over-all efficiency of all counters was then found to be better than 95%. The ratio of the average pulse heights at the best and worst points on the counters varied between two and four.

A scale drawing showing the position of the ring counters with respect to the hydrogen target is given in Figure 10. Each ring counter overlaps the adjacent one in order to improve the angular definition. It took one or two consecutive counts from each of the two cones of counters to define the scattering angle of the K^+ meson to better than $\pm 5^\circ$. Each of the chosen counter combinations then detected scattering events occurring at some particular volume inside the target only, and

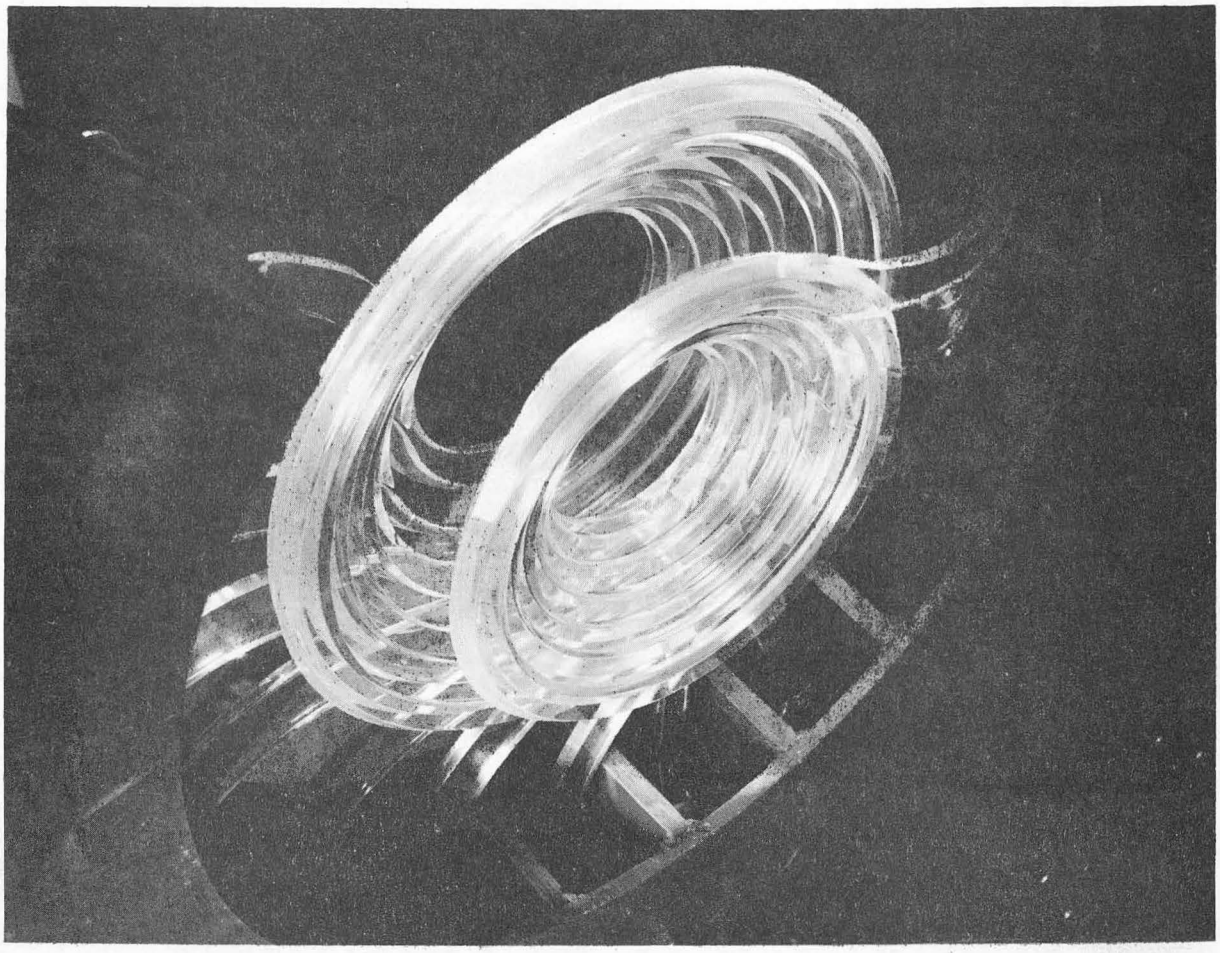

ZN-2154

Fig. 9. Photograph of the 15-ring counters.

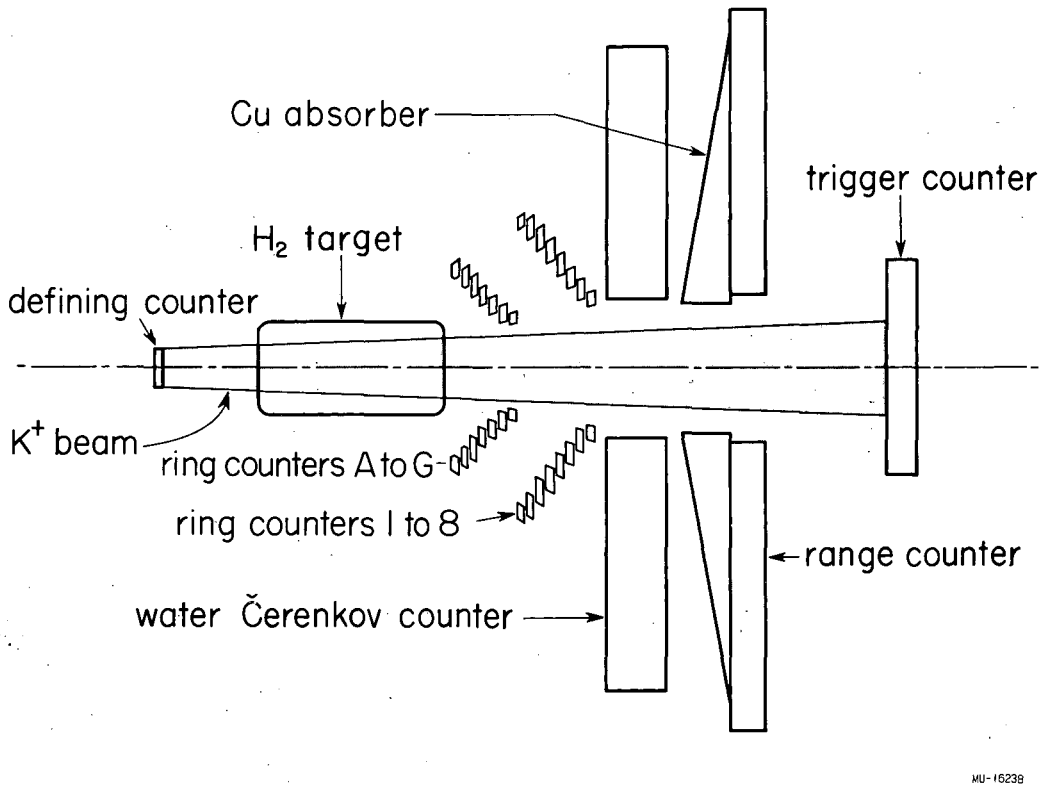

Fig. 10. Cross-sectional diagram of the target and scattering-detection counters.

did not "see" the defining counter D, or the Mylar and steel windows of the target. It was possible for some of the selected counter combinations to detect scattering events in the walls of the Mylar vessel containing the liquid hydrogen, but these walls were very thin and their effect (determined by running the target empty) could be subtracted out.

D. K^+-Meson-Decay Background

The percentage of K^+ mesons that decay inside the 6-in. long target is given by

$$P = \left(1 - e^{\frac{-x}{\beta c \gamma \tau}}\right) \times 100 \ , \qquad (2)$$

where $\beta c = 2.19 \times 10^{10}$ cm/sec , the velocity of the K^+ meson;

$\tau = 1.22 \times 10^{-8}$ sec , the mean life of a K^+ meson in its rest frame;

$\gamma\tau = 1.78 \times 10^{-8}$ sec , the mean life of a K^+ meson moving with velocity βc;

$x = 15.2$ cm , the length of the target.

By inserting these numbers into Eq. (2), one find P = 3.6%. The branching ratios for the various decay modes of the K^+ meson are given in Table III.[6] The dominant decay modes, $K_{\pi 2}$ and $K_{\mu 2}$, are of the two-body type, in contrast to the rarer K_γ, $K_{\gamma'}$, $K_{\mu 3}$, and K_{e3} three-body decays. Except for the K_γ decay mode, in which the three secondaries are charged, any of the other decays in the target would appear to be a scattering event if the charged decay product went forward into a cone of half angle 50°. The decay events then would be a background that would be about four times the effect being investigated. In order to obtain a differential scattering cross section with reasonable

statistics it was necessary to eliminate the confusion of scattering events with decays.

Table III

K^+-meson decay modes	
Type	Abundance (%)
$(K^+_\tau) \rightarrow \pi^+ + \pi^+ + \pi^-$	5.56 ± 0.41
$(K^+_{\tau'}) \rightarrow \pi^+ + \pi^0 + \pi^0$	2.15 ± 0.47
$(K^+_{\mu 2}) \rightarrow \mu^+ + \nu$	58.2 ± 3.0
$(K^+_{\pi 2}) \rightarrow \pi^+ + \pi^0$	28.9 ± 2.7
$(K^+_{\mu 3}) \rightarrow \mu^+ + \nu + \pi^0$	2.83 ± 0.95
$(K^+_{e 3}) \rightarrow e^+ + \nu + \pi^0$	3.23 ± 1.3

Figure 11 shows, as a function of laboratory-system angle, the variations in laboratory-system velocity of the scattered K^+ meson, the recoil proton, the π^+ meson from $K_{\pi 2}$ decay, and μ^+ from $K_{\mu 2}$ decay. The two predominant decay modes could then easily be identified by their velocity; this identification was the purpose of the water Cherenkov counter. It detected particles with a velocity β greater than 0.75. Clearly, for all the $K_{\pi 2}$ and $K_{\mu 2}$ decay modes the charged secondary going into the forward cone of half angle 50^0 would have a high enough β to count. The positron from K_{e3} decay would have a β of almost 1 for all forward angles and should count without difficulty. In the K^+_τ decay there was a large probability that one of the three π's would count in the Cherenkov counter. Left were the $K_{\mu 3}$ and $K_{\tau'}$ decay modes in which

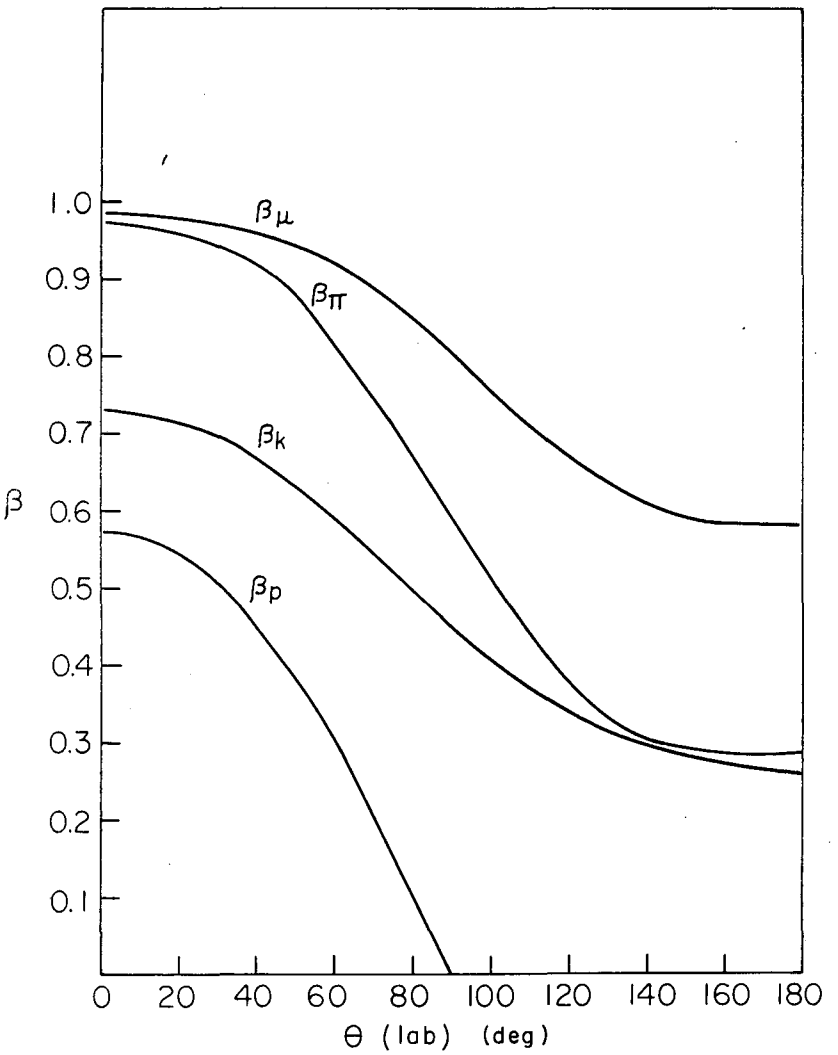

Fig. 11. The variation of β as a function of θ (lab) of the π and μ meson from $K\pi_2$ and $K\mu_2$ decay in flight (for a K^+-meson kinetic energy of 225 Mev) and of the recoiling proton and scattered K^+ meson.

the charged secondary had a spread in β for each laboratory-system angle. The two modes composed only 5% of all the decay modes, and more than 65% of the forward-going charged secondaries had a $\beta > 0.80$. Thus, less than 2% of the decays would act as background.

The angular distribution for decay modes with a single charged secondary with $\beta > 0.8$ is given later in a section on the calibration of the ring counters.

E. Water Cherenkov Counter

The water was contained in a cell made of Lucite 1/16 in. thick. The cell was disc-shaped, 21 in. in diameter and 1-7/8 in. thick, with fourteen 1/4-in. diameter Lucite studs cemented between the two large flat sheets to give it strength. A sealed-off hole, 4.5 in. in diameter, in the center (as shown in Fig. 10), allowed free passage of the unscattered K^+ mesons. Fifteen 6655 RCA-type photomultiplier tubes were arranged around the outer circumference. Such a large number of tubes was used to ensure a high counting efficiency over the very large volume of the counter. A light shifter was used to increase the number of photons in the frequency interval to which the photomultiplier tube is sensitive. The shifter consisted of 2-amino-6, 8-naphthalene-disulfonic acid disodium salt, in a concentration of 10 mg per liter. According to Heiberg and Marshall, the effect of the shifter on their water Cherenkov counter was to increase the pulse height by about 30%.[7]

A layer of magnesium oxide 1/8 in. thick was set on the inside of the aluminum sheets used to cover the counter. Magnesium oxide is an excellent reflector even in the ultraviolet region, and as it was not in

optical contact with the Lucite cell, the advantages of critical reflections were not sacrificed. A special technique was developed for the formation of such thick coatings of MgO without destroying its high reflectivity.[8]

The counter was checked by inserting it behind the defining counter and passing the particles in the K^+ beam through it. The counter telescope was first timed for π^+ mesons which had a velocity β of 0.97, and the π_β counter was turned off. The oscilloscope was triggered by the π^+-meson pulse and the amplified output of the Cherenkov counter displayed on the sweep. The unsaturated Cherenkov pulses were relatively uniform in height, indicating a very high light-collecting efficiency. When the counter telescope was then timed for protons which had a velocity β of 0.49 and a similar test was made, no pulses could be seen. This indicated that the light shifter was not scintillating to any detectable extent.

F. Separation of Scattered K^+ Mesons from Recoil Protons

The separation was achieved by range.[9] Figure 12 shows the limits in the spread in range of both particles in copper as a function of the laboratory-system angle of the particle. The range spread is due to the $\pm$ 25-Mev energy spread of the incident K^+ mesons. It is apparent from Fig. 12 that, for the K^+ beam with a kinetic energy of 225 $\pm$ 25 Mev at the center of the target, the slowest K^+ meson corresponding to an initial K^+-meson energy of 200 Mev had a greater range in copper than the proton recoiling from a collision with a 250-Mev K^+ meson for all angles from 0° to 50° (lab). It was sufficient, then, to insert behind

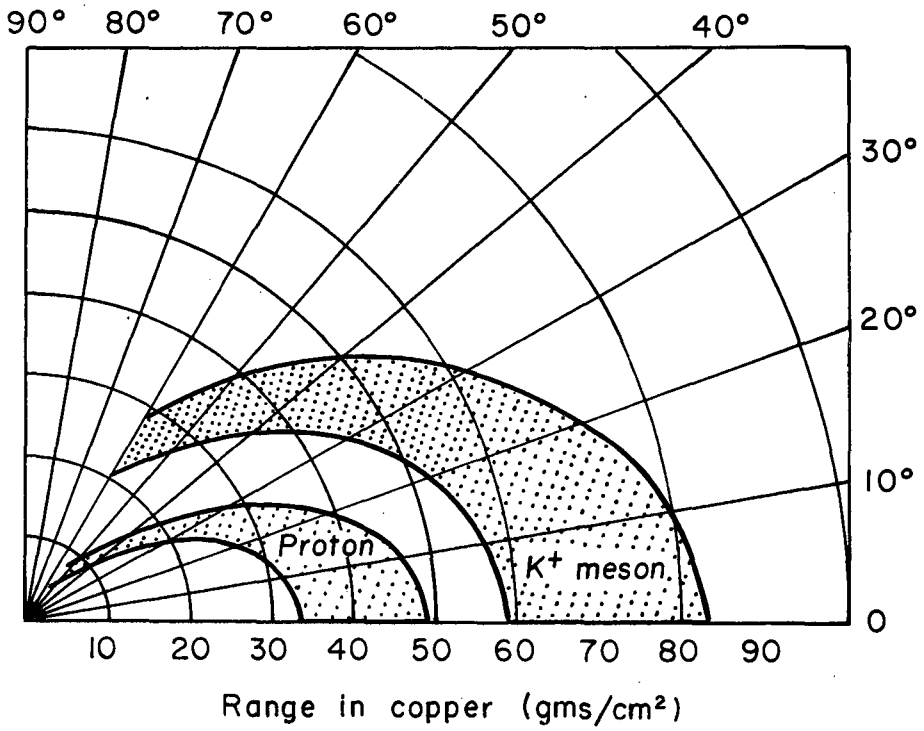

Fig. 12. Range distribution in copper of 225 ± 25 - Mev K^+ mesons and recoiling protons.

the water Cherenkov counter a copper disc with the thickness dropping off with increase in radius in just the right way to stop all the protons and let the K^+ mesons through. A large scintillation counter (range counter) behind the copper disc could then detect the K^+ mesons scattered forward and passing through the copper. The arrangement is seen in the scale drawing in Fig. 10. The range-energy relationships that were used were based on the proton range-energy tables given by Aron,[10] but extracted from a report by Atkinson and Willis.[9] The energy of the K^+-meson beam was also determined by range in copper, so that even if the range-energy curves were not quite correct, the error would tend to cancel.

G. The Scattering-Range Counter

The range counter consisted of four separate quadrant counters which, when put together, formed a circular disc 23½ in. in diameter with a center hole 4-3/4 in. in diameter. The counters were 1 in. thick and were certain of having a high counting efficiency. The four anode outputs were added to form a single output of the "range counter."

H. Electronics for the Detection and Recording of Scattering Events

A block diagram of the electronics is shown in Fig. 13. The pulses from the ring counters were limited in the amplifiers, attenuated to 0.8 volt, and delayed. The water Cherenkov counter required an additional amplifier, everything else being the same, while the range counter and trigger counter required only one amplifier each.

The origin of the S_2 and C_3 outputs entering the system in Fig. 13

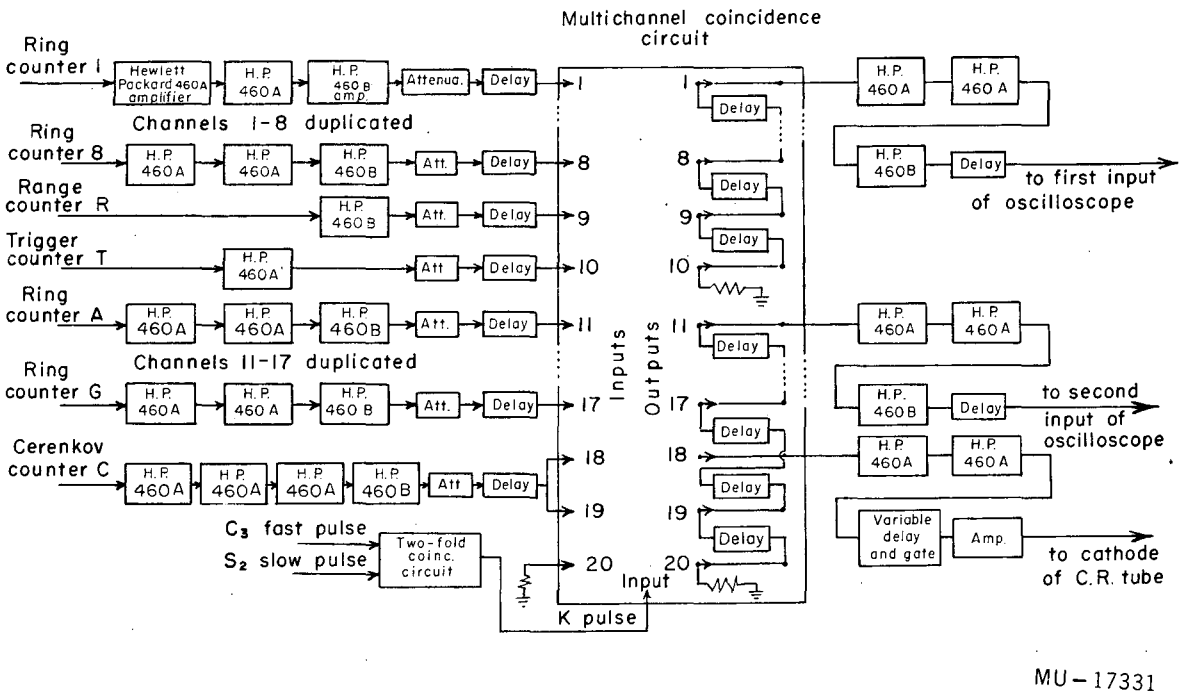

Fig. 13. Block diagram of the electronics associated with the scattering detection counters.

is shown in Fig. 3. Since the 10^{-7}-sec S_2 pulse required the existence of the 10^{-8}-sec C_3 pulse, the purpose of taking a coincidence between them was to obtain a short 10^{-8}-sec K^+ pulse, also 0.8 volt high.

Coincidences were taken between the K^+ pulse and each of the 18 counter outputs. This was done by means of 20 twofold diode coincidence circuits as shown in Fig. 13. Outputs from ring counters Nos. 1 to 8, the range counter, the trigger counter, and ring counters A to G, in that order, were connected to the inputs of Channels 1 to 17. The output of the Cherenkov counter was connected to both Channels 18 and 19. Channel 20 was terminated at the input and a diode removed from it to allow the K^+ pulse to feed through to the output. The output of Channel 20 would act as a timing or line-up pulse for the identification of the other output pulses. The outputs of coincidence Channels Nos. 1 to 10 were delayed with respect to one another with 50 feet of RG-63/U cable, or 6×10^{-8} sec. Channel 10 output was terminated with a 125-Ω resistor and the coincidence pulses were taken through Channel 1 output, amplified, delayed, and displayed on one of the two sweeps that were used of a four-gun cathode-ray tube. Outputs of Channels 11 to 20 were delayed in a similar way with respect to one another except for the output of Channel 18, which was skipped and 12×10^{-8} sec. delay inserted between the Channel 17 and Channel 19 outputs. The 125-Ω terminating resistor was at Channel 20 output, and the coincidence outputs were taken through Channel 11, amplified, delayed, and displayed on the second sweep of the cathode-ray tube, a description of which follows.

The model 517 Tektronix oscilloscope had mounted on it a four-gun

cathode-ray tube unit described in UCRL Drawing No. 2X2765H. Incorporated in this unit is a vertical sweep stepper described in UCRL Drawing No. 2X693. The output of Channel 18 was amplified and then used to trigger a delay and gate unit described in UCRL Drawing No. 2X643H. The 20-volt, 10^{-6}-sec. output pulse of the gate went through an amplifier to the cathode to blank the sweep. This method was more advantageous than an additional anticoincidence circuit. The blanking was turned off for 5- to 10-minute intervals about every 2 hours in order that we might obtain a calibration of the ring counters by comparing the experimental angular distribution of the charged decay products to the predicted distribution.

The problem of photographing as many as five events occurring in rapid succession was solved by vertically displacing the traces on successive events. This was done with a vertical sweep stepper, triggered by the oscilloscope sweep, and reset by a Bevatron timing pulse shortly before the spilling of the proton beam on the production target. The sweeps were photographed with a Type 321-A Dumont Oscillograph Record Camera at a film drive speed of $2\frac{1}{2}$ in. per minute.

IV DETERMINATION OF THE TOTAL K^+-p CROSS SECTION

A. Scaler Data

The total cross sections of K^+ mesons on protons at the three energies of 175±25 Mev, 225±25 Mev, and 275±25 Mev were obtained from the $\bar{S}$ and S_2 scaler readings. The S_2 readings gave the number of K^+ mesons passing through D, the defining counter, whereas the $\bar{S}$ reading gave the number of K^+ mesons that passed through the defining counter but did not reach T, the trigger counter. The $\bar{S}$ and S_2 readings were accumulated for "target full" and "target empty" for each of the three energies. Table IV lists these numbers as well as the ratios of $\bar{S}/S_2$, which are the fractions of K^+ mesons removed from the K^+ beam.

Table IV

Summary of scaler readings

Scaler	Energy (Mev)		
	175 ± 25	225 ± 25	275 ± 25
$\bar{S}\|_f$ (target full)	68,195	105,646	34,684
$S_2\|_f$	415,582	742,672	275,308
$\bar{S}\|_e$ (target empty)	68,063	44,944	30,014
$S_2\|_e$	442,917	338,033	258,375
$\frac{\bar{S}}{S_2}\|_f$	0.1640	0.14225	0.1259
$\frac{\bar{S}}{S_2}\|_e$	0.1536	0.13295	0.1161

The total scattering cross section is a small effect obtained from the difference of two relatively large quantities, namely $\left.\frac{\bar{S}}{S_2}\right|_f$ and $\left.\frac{\bar{S}}{S_2}\right|_e$. The relative statistical error on the difference of the ratios could be as low as 10% only because so many K^+ mesons were used at each energy.

B. <u>The Corrected Total K^+-p Cross Section</u>

The K^+ mesons are removed from the beam by the decay and scattering processes according to

$$dN(x) = -N(x)(\lambda_s(x) + \lambda_D(x))\,dx, \qquad (3)$$

where $dN(x)$ is the drop in the number of K^+ mesons per cm^2 in the beam in a distance dx.

$N(x)$ is the number of K^+ mesons per cm^2 in the beam at point x,

$\lambda_D(x)$ is the reciprocal decay length for decays in which the charged decay products miss the T counter,

and $$\lambda_s(x) = n(x)\,\sigma(x), \qquad (4)$$

where $n(x)$ is the number of scattering centers per cm^3 at x,

$\sigma(x)$ is the scattering cross section at x for scattering events with angles large enough to miss the T counter.

Integrating Eq. (3), we get

$$\frac{N(x_1)}{N(x_0)} = \exp\left\{-\int_{x_0}^{x_1} (\lambda_s(x) + \lambda_D(x))\,dx\right\} . \qquad (5)$$

where x_0 is taken to be a point immediately before the defining counter D,

$N(x_0) = S_2$,

x_1 is a point at which the trigger counter is situated,

and $N(x_1) = S_1 = S_2 - \bar{S}$.

The integration in Eq. (5) over x is performed for target full and target empty, for which the ratio $\frac{N(x_1)}{N(x_0)}$ becomes $\left(1 - \frac{\bar{S}}{S_2}\right)_f$ and $\left(1 - \frac{\bar{S}}{S_2}\right)_e$ respectively.

By subtracting these two expressions of Eq. (5) we get

$$\frac{\bar{S}}{S_2}\Big|_f - \frac{\bar{S}}{S_2}\Big|_e = \exp\left\{-\int_{x_0}^{x_1} (\lambda_S(x) + \lambda_D(x))\,dx\right\}_e - \exp\left\{-\int_{x_0}^{x_1} (\lambda_S(x) + \lambda_D(x))\,dx\right\}_f$$

The integrals over x can be broken up into regions before the target, inside the target, and after the target. Since the scattering events and decays before the target will be the same for both "target full" and "target empty," the integrals over those regions will be identical.

For the interval inside the target, account had to be taken of the scattering off the hydrogen gas in the target for the "target empty" case. The hydrogen gas density at that temperature was about 2% of the liquid density. In the region after the target the integrals are not similar. This is mostly because of the additional drop in K^+-meson momentum for "target full." The reciprocal decay length λ_D due to the latter effect is almost 2% larger for "target full" than for "target empty." This difference is almost 10% as large as the effect due to K^+ mesons scattering off the protons in the target. Account was taken of this decay correction, which tended to lower the total K^+-meson-proton cross section, and the extent of the correction differed according to K^+-meson momentum. The scatterings in the walls behind the target were similar for "target full" and "target empty."

Contamination of the K^+-meson beam by its charged decay products

was insignificant because the decays occur predominantly at larger angles.

The results of the quantitative calculations (given in Appendix A) are contained in Table V.

Table V

Corrected total K^+-p cross sections from scaler data

Energy (Mev)	Total K^+-p cross section (mb)
175 ± 25	16.3 ± 1.7
225 ± 25	15.2 ± 1.3
275 ± 25	16.3 ± 1.7

V DETERMINATION OF THE DIFFERENTIAL K^+-p CROSS SECTION

A. Film Reading and Sorting of Events

The film on which the sweeps were recorded was projected on an outline of the two sweeps identifying the various pulses by their position with respect to the K pulse. This process is represented in Fig. 14. The first ten channels are displayed on the top sweep and the second ten channels on the bottom one. The particular event shown implies that a K^+ meson scattered forward (deduced from the R pulse) at a laboratory-system angle of $30° \pm 5°$ (deduced from the 4, 5, and D ring counter pulses). It was not a K^+-meson decay, because neither did C, the Cherenkov counter pulse, appear, nor were the sweeps blanked out. However, a K^+-meson decay event did occur shortly after the scattering event, and it also is seen in Fig. 14. The stepper displayed upwards the second set of sweeps, but the delay and gate unit blanked the sweep out shortly after it began.

Scanners read the film and recorded all the events. Out of these readings all the possible scattering events and decay events were selected and punched out on IBM cards separately. The IBM 650 computer was programmed to read the cards and to tally up the events in their designed memory locations, and, in the end, to read out the tallies. This was done for "target full" and "target empty" data, with results as given in Appendix B.

A negligible fraction of the sweeps was not read, because of superposition of sweeps or loss of film. An effective S_2, which is the number

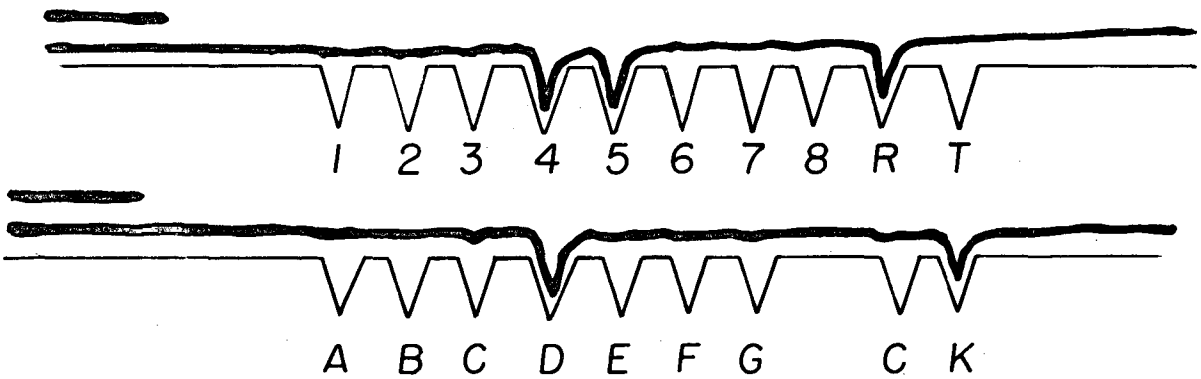

MU-17323

Fig. 14. A sample scattering event represented by the combination of the two traces. The pulses from counters 4, 5, D, and R indicate a forward scattering (deduced from the R pulse) at a lab angle of $30^{\circ} \pm 5^{\circ}$ (deduced from the 4, 5, and D pulses).

of incident K^+ mesons that corresponded to the data given in Appendix B, was obtained from the relationship

Effective $S_2 = (S_2/\bar{S}) \cdot$ (number of sweeps read).

The effective S_2's (abbreviated as eff. S_2) were computed for each run, and summed for "target full" and "target empty" data (and are given in Appendix B). The extent of the background for each counter combination is evident upon comparison of the number of counts for "target empty" and "target full."

B. Calibration of the Ring Counters

The ring counters were calibrated by comparing the experimentally determined decay distribution with the theoretical one for each counter combination. The theoretical decay distribution is calculated in Appendix C.

The fraction of K^+ mesons that decay and count in a particular counter combination is

$$\frac{N}{N_0}\Big|_D = \int_\theta P_D(\theta) \cdot P_c(\theta) \in d\theta \quad . \tag{8}$$

where N is the number of decays counted in that counter combination,

N_0 is the effective S_2 for decay, or the effective number of incident K^+ mesons,

$P_D(\theta)$ is the probability per radian per centimeter of travel that a K^+ meson will decay at an angle θ and count in the water Cherenkov counter,

$P_c(\theta)$ is the probability, in units of centimeters, that the counter combination will detect the decay,

and ϵ is a factor that accounts for the calibration and efficiency of the counter combination.

We have $P_D(\theta) = \frac{1}{\beta c \gamma \tau} \cdot \frac{1}{N_o} \frac{dN}{d\theta}$, (9)

where $\beta c \gamma \tau = 390\ cm$,

and $\frac{1}{N_o}\frac{dN}{d\theta}$ is given in Appendix C as a function of θ ,

$P_c(\theta) = \ell_D$, the distance along the axis of the target within which a decay at angle θ would count in the counter combination 12AB.

We can rewrite the expression for $\left.\frac{N}{N_o}\right|_D$ as

$$\left.\frac{N}{N_o}\right|_D = \int_\theta \frac{1}{\beta c \gamma \tau} \cdot \frac{1}{N_o}\frac{dN}{d\theta} \cdot \ell_D \cdot \epsilon \cdot d\theta$$

$$= \frac{1}{\beta c \gamma \tau} \cdot \left\langle \frac{1}{N_o}\frac{dN}{d\theta} \right\rangle \cdot \epsilon \int_\theta \ell_D \, d\theta, \qquad (10)$$

where $\left\langle \frac{1}{N_o}\ \frac{dN}{d\theta} \right\rangle$ implies that the quantity was averaged over the angle θ .

This expression is now used to determine ϵ , which enters into the expression for the differential cross section.

As an example, ϵ will be computed for ring counter combination 12AB which counted 33 decays out of an effective S_2 of 119,038. The distance ℓ_D as a function of angle was determined graphically (ℓ_D may extend outside of the hydrogen target). To simplify the procedure it was assumed that the decay secondary lay in the plane formed by the axis of the target and the track of the incident K^+ meson, i.e., that the azimuthal angle ϕ was zero. This was a very conservative assumption, since the K^+ beam was much smaller in diameter than the ring counters. The variation

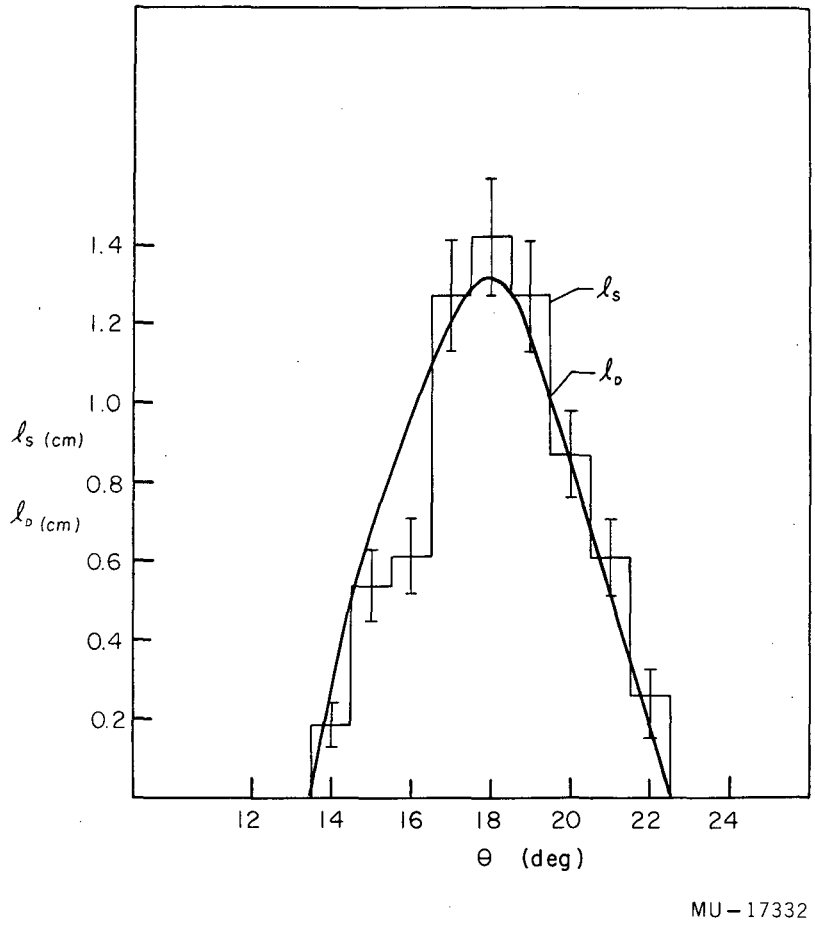

Fig. 15. The (ℓ_D) is the probability (in units of centimeters) that the counter combination 12 AB will detect the decay at angle θ . The (ℓ_S) is the probability (in units of centimeters) that the counter combination will detect the scattering occurring at angle θ.

in ℓ_D as a function of θ is given in Fig. 15. The area under the curve was measured and found to be 0.126 cm radians. The value of $\frac{1}{N_0}\frac{dN}{d\theta}$, obtained from Fig. C3, was 0.825 at 18° (lab), at which the peak in ℓ_D occurs. We now have sufficient information to determine ϵ:

$$\epsilon = \frac{\frac{N}{N_0}\Big|_D \cdot \beta \kappa \gamma T}{\left\langle \frac{1}{N_0}\frac{dN}{d\theta} \right\rangle \cdot \int_\theta \ell_D \, d\theta} \qquad (11)$$

$$= \frac{\frac{33}{119{,}038} \cdot 390}{0.825 \times 0.126} = 1.04$$

C. Calculation of the Cross Section

In a similar way the fraction of K^+ mesons that scatter off the protons and count in 12 AB is

$$\frac{\bar{S}}{\text{eff } S_2}\Big|_f - \frac{\bar{S}}{\text{eff } S_2}\Big|_e = \int_\theta P_s(\theta)\, P_c'(\theta)\, \epsilon \, d\theta \qquad (12)$$

where $\frac{\bar{S}}{\text{eff } S_2}\Big|_f - \frac{\bar{S}}{\text{eff } S_2}\Big|_e$, which is the difference between "target full" and "target empty" effects, gives the effective fraction of K^+ mesons scattering off protons,

$P_s(\theta)$ is the probability per radian per centimeter of travel that a K^+ meson will scatter at angle θ,

$P_c'(\theta)$ is the probability, in units of centimeters, that the counter will detect the scatter,

and ϵ has been defined previously.

We have $P_s(\theta) = n \left.\frac{d\sigma}{d\theta}\right|_L \ (\text{rad}^{-1})$ (13)

where n is the number of protons per cm^3, and

$\left.\frac{d\sigma}{d\theta}\right|_L$ is the laboratory-system differential cross section for the scattering of K^+ mesons off protons,

$P_c'(\theta) = \ell_s$ is the length of the target within which a scattering event at angle θ counts in the counter combination 12 AB.

By rewriting Eq. (12) we obtain

$$\left.\frac{\bar{S}}{\#S_2}\right|_f - \left.\frac{\bar{S}}{\#S_2}\right|_e = \int_\theta n \left.\frac{d\sigma}{d\theta}\right|_L \ell_s \epsilon \, d\theta$$

$$= n \left\langle \left.\frac{d\sigma}{d\theta}\right|_L \right\rangle \epsilon \int_\theta \ell_s \, d\theta \qquad (14)$$

The laboratory-system differential cross section $\left\langle \left.\frac{d\sigma}{d\theta}\right|_L \right\rangle$ at angle θ can be determined once $\int_\theta \ell_s d\theta$ is known. This integral will not agree with $\int_\theta \ell_0 d\theta$ for counter combinations which "see" the K^+ beam ahead of or behind the target.

The quantity ℓ_s was not determined graphically as ℓ_D was, but instead was obtained by the Monte Carlo method on the IBM 701 computer. The reason for obtaining ℓ_s on the computer was because of the additional complexity of the problem. It was necessary to know, for K^+-meson scatterings between 35° and 65° (lab), the fraction of the time that both the scattered K^+ meson and the recoil proton counted in the ring counters. These events were discarded in the selection of scattered events and would have introduced a bias against scatterings in that angular interval. The quantity ℓ_s was determined in the following way:

One thousand scatters were simulated by the computer at each angle in 1-degree steps at random positions and at random azimuthal angles

inside the hydrogen target. The quantity ℓ_s for a given counter combination and a given angle is expressed by

$$\ell_s = h\ell/1000, \tag{15}$$

where h is the number of counts obtained for that counter combination for the particular angle, and

ℓ is the length of the target in centimeters.

The results and statistical errors obtained for ℓ_s are shown in Fig. 15 for comparison with ℓ_D. The area under the histogram is equivalent to $\int_\theta \ell_s \, d\theta$ and is equal to 0.122 ± 0.006 cm radian, in very good agreement with 0.126 for $\int_\theta \ell_0 \, d\theta$.

The effective proton density n is equal to $\frac{98}{100}$ x 0.07 x 6.023 x 10^{23}cm^{-3} after correction for the density of hydrogen gas in the target for "target empty."

The difference $\frac{\bar{S}}{\text{eff } S_2 \text{ f}} - \frac{\bar{S}}{\text{eff } S_2 \text{ e}}$ is found to be 0.247 x 10^{-4}, from the data in Appendix B.

An expression for the differential cross section $\left\langle \frac{d\sigma}{d\theta}\Big|_L \right\rangle$ is obtained from Eq. (14).

$$\left\langle \frac{d\sigma}{d\theta}\Big|_L \right\rangle = \frac{\overline{\text{eff } S_2}\big|_f - \overline{\text{eff } S_2}\big|_e}{n \, \epsilon \int_\theta \ell_s \, d\theta} \tag{16}$$

$$= \frac{0.247 \times 10^{-4}}{0.414 \times 10^{23} \times 1.04 \times 0.122}$$

$$= 4.7 \text{ mb/radian}$$

$$\text{and } \left\langle \frac{d\sigma}{d\Omega}\Big|_L \right\rangle = \frac{4.7}{2\pi \sin 18^\circ} = 2.4 \text{ mb/steradian} \tag{17}$$

Upon transformation to the center-of-mass system, the differential cross section becomes

$$\left\langle \frac{d\sigma}{d\Omega}\Big|_{c.m.} \right\rangle = 2.4 \frac{d\sigma_2}{d\Omega_{c.m.}} = 0.95 \pm 0.70 \text{ mb/steradian} \quad (18)$$

The large statistical error on $\frac{d\sigma}{d\Omega}\Big|_{c.m.}$ arises from $\frac{\bar{S}}{S_2}\Big|_f - \frac{\bar{S}}{S_2}\Big|_i$. If written in units of λ^2, the differential cross section becomes

$$\frac{1}{\lambda^2} \frac{d\sigma}{d\Omega}\Big|_{c.m.} = 0.24 \pm 0.18 \text{ per steradian}, \quad (19)$$

and corresponds to the center-of-mass scattering angle of 30°.

For backward scatterings in which the proton recoils forward, a somewhat similar treatment was followed.

More than 100 counter combinations were used to obtain the differential cross-section data. Counter combinations were grouped together into ± 10° angular intervals in the center-of-mass frame of reference and the calculations shown above were performed on the groups. It was then necessary to estimate the corrections on these results.

D. Corrections

The numerous small corrections that must be applied to the differential cross section are categorically discussed below.

Account had to be taken of the K^+ mesons that scattered backwards, came to rest, decayed, and counted in the water Cherenkov counter. The loss of events due to this effect amounted to 7% for scatterings at angles greater than 125° in the laboratory system.

A second correction accounted for a 6 to 7% loss of the forward-scattered events due to K^+-meson decays, after scattering, which are

counted in the Cherenkov counter.

Still another correction accounted for the decrease in K-meson flux in the target. The correction varied from an increase of 4% at 40° and 140° to an increase of 5.5° at 80° (c.m.).

Another important correction is due to K^+ mesons that interact and come to rest in the copper, but count in neither the Cherenkov counter nor the range counter. The loss here varied from 8% at 20° to 5% at 60° (c.m.). These events looked like backward scatterings and therefore the backward differential scattering cross section had to be lowered by the right amount to bring it to the correct value.

A final small correction is due to K^+ mesons that come to rest in the range counter at angles near 50° (lab), decay, and count in the Cherenkov counter. This accounted for less than 1% loss in the scatterings.

It was not necessary to correct for the 7% total accidental rate in the ring counters in the counter detection system. Events that are thrown out due to accidental counts make the ring counter combinations appear less efficient, and this has already been corrected for with the quantity ϵ .

A composite correction due to the above-mentioned effects as a function of the c.m. angle is given in Fig. 16. The quantity C gives the fraction of events at each angle that are counted.

E. The Corrected Differential K^+-p Scattering Cross Section

The differential cross section obtained from calculations as shown in Section C, when divided by the curve in Fig. 16, gave the corrected

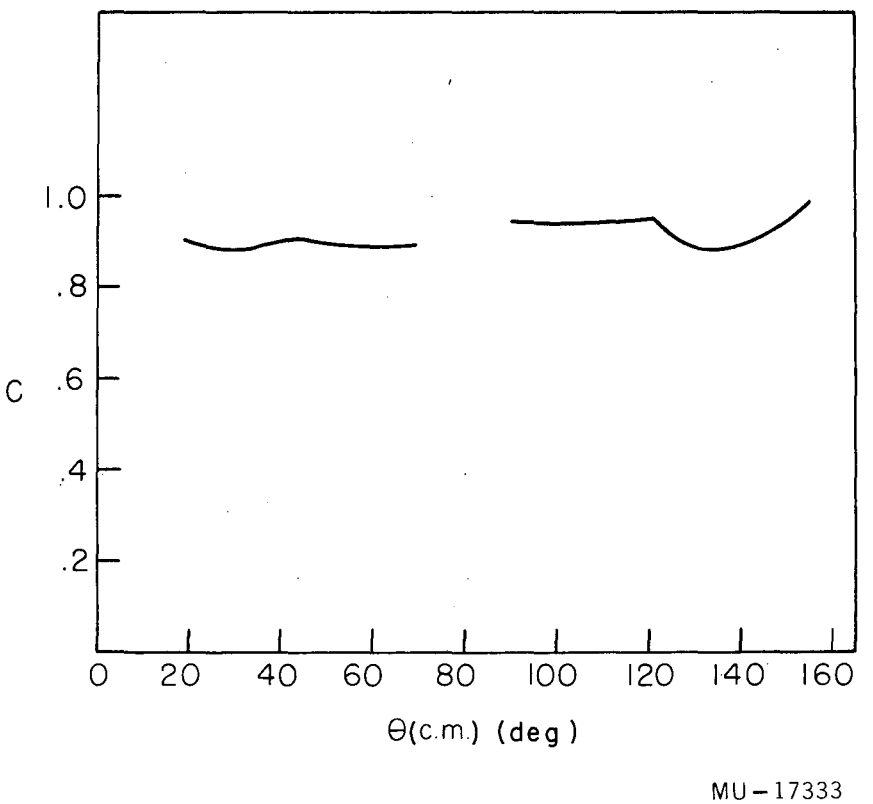

Fig. 16. Composite correction that gives the fraction of the events at each angle that are counted.

differential-cross-section points in Fig. 17. The cross section was peaked at small angles in the forward direction but, aside from this, there was no pronounced asymmetry within the statistical errors in the angular distribution. The lack of data in the angular interval from 70° to 90° was due to the confusion created because both scattered K^+ mesons and recoil protons were counted in the ring counters. By integrating the differential-cross-section curve over $\theta_{c.m.}$ we obtained an absolute total cross section σ_T of $9.5\,\lambda^2$ or 15.3 mb. This agrees very well with the total cross section of 15.2 ± 1.3 mb obtained from scaler data--as it should. The two numbers are not statistically independent, however, since one-third of the same events used to obtain σ_T from scaler data was used to obtain the differential cross section $\frac{d\sigma}{d\Omega}$. The fraction is as low as a third because the ring counters would not "see" any of the large-angle scatterings occurring at the forward half of the target.

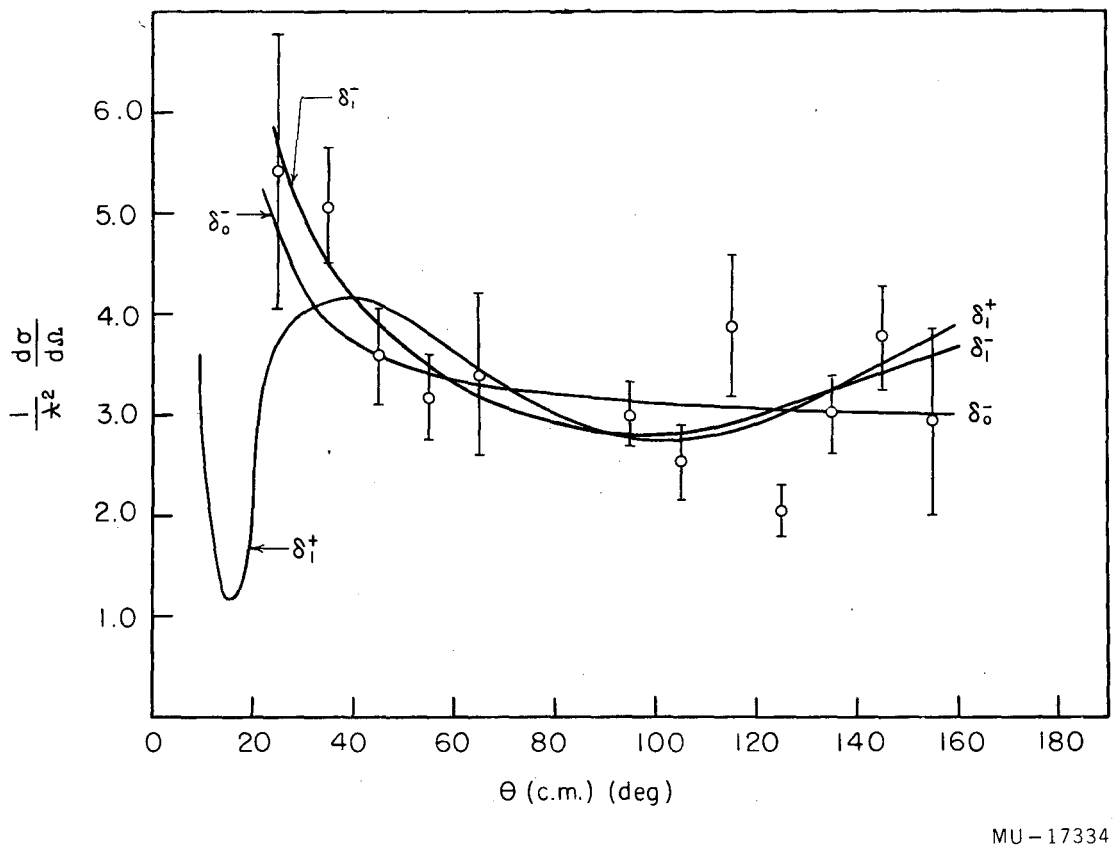

Fig. 17. The differential-scattering cross sections and three possible phase-shift combinations that are fitted to the data; δ_0^- corresponds to virtually pure $s_{\frac{1}{2}}$-wave scattering with a repulsive K^+-p potential; δ_1^- and δ_1^+ correspond to virtually pure $p_{\frac{1}{2}}$-wave scattering with a repulsive and an attractive K^+-p potential respectively.

VI PHASE-SHIFT ANALYSIS

The angular distribution of the scattering of K^+ mesons from protons was analyzed in terms of the angular-momentum states involved. We assumed that the compound K^+-meson-nucleon states responsible for the scattering were $s_{\frac{1}{2}}$, $p_{\frac{1}{2}}$, and $p_{\frac{3}{2}}$, and that states of higher angular momentum offered little or no contribution. From the assumption of charge independence for the nuclear interaction between the K meson and nucleon, it followed that K^+ mesons scattered from protons in a pure T=1 isotopic spin state. The number of phase shifts necessary to describe the differential cross section was thus reduced to three, namely δ_0, δ_1, and δ_3 for scattering in the $s_{\frac{1}{2}}$, $p_{\frac{1}{2}}$, and $p_{\frac{3}{2}}$ states, respectively. It is possible to determine experimentally the absolute signs of the phase shifts from the interference of the nuclear scattering with some other scattering of known sign, such as Coulomb scattering. Since the Coulomb scattering of K^+ mesons from protons is repulsive, a constructive interference would prove a repulsive nuclear interaction.

The differential cross section in the center-of-mass system for scattering without and with spin flip and including the Coulomb effect is [11]

$$\left.\frac{d\sigma}{d\Omega}\right|_{nf} = \frac{\lambda^2}{4}\left| \frac{-i\gamma\alpha}{\sin^2\frac{\theta}{2}}\, e^{-i\gamma\alpha \log \sin^2\frac{\theta}{2}} + P + Q\cos\theta \right|^2 \qquad (20)$$

$$\left.\frac{d\sigma}{d\Omega}\right|_{f} = \frac{\lambda^2}{4}\left| R^2 \right| \sin^2\theta, \qquad (21)$$

where $\gamma = 1$ for K^+-p scattering,

$\lambda\!\!\!^{-}$ is the de Broglie wave length of the K^+ meson in the center-of-mass system,

$$\alpha = \frac{\mu e^2 \lambda\!\!\!^{-2}}{\hbar^2 (1-\beta^2)^{\frac{1}{2}}},$$

where μ, e, and $\hbar$ are the reduced mass of the K^+-meson-proton system, the charge, and Planck's constant respectively,

β is the velocity of the K^+ meson relative to the proton,

$$P = e^{2i\delta_0} - 1 = \sin\delta_0 e^{i\delta_0}, \tag{22a}$$

$$Q = \frac{1+i\alpha}{1-i\alpha}\left[\sin\delta_1 e^{i\delta_1} - 2\sin\delta_3 e^{i\delta_3}\right], \tag{22b}$$

$$R = \sin\delta_3 e^{i\delta_3} - \sin\delta_1 e^{i\delta_1}. \tag{22c}$$

Some simplification is possible. For a K^+-meson energy of 225 mev (lab), $\alpha = 0.014$. It can thus be neglected in Q without contributing more than 3% uncertainty in the scattering amplitude. The expression $\exp(-i\gamma\alpha \log\sin^2\frac{\theta}{2})$ can be reasonably well approximated by unity for $\theta > 20^\circ$, for which $\alpha \log\sin^2\frac{\theta}{2} < 0.002$.

The combination of the differential cross sections for scattering without and with spin flip in units of $\lambda\!\!\!^{-2}$ is

$$\frac{1}{\lambda\!\!\!^{-2}}\frac{d\sigma(\mu)}{d\Omega} = \left\{\left|\frac{1-i\alpha}{1-\mu} + \sin\delta_0 e^{i\delta_0} + (\sin\delta_1 e^{i\delta_1} + 2\sin\delta_3 e^{i\delta_3})\mu\right|^2 + \left|\sin\delta_3 e^{i\delta_3} - \sin\delta_1 e^{i\delta_1}\right|^2 (1-\mu^2)\right\}, \tag{23}$$

where $\mu = \cos\theta$.

A good fit of $\frac{1}{\lambda^2}\frac{d\sigma(\mu)}{d\Omega}$ to the experimentally determined differential cross sections corresponds to minima in

$$\chi^2 = \sum_i \left(\frac{y(\mu_i) - \frac{1}{\lambda^2}\frac{d\sigma(\mu_i)}{d\Omega}}{\sigma(\mu_i)} \right)^2, \qquad (24)$$

where $y(\mu_i)$ and $\sigma(\mu_i)$ are the experimental cross sections and their statistical errors. The method of minimizing χ^2 is briefly described in Appendix D. Three phase-shift combinations, δ_0^-, δ_1^-, and δ_1^+, which were found to give significant minima, are listed in Table VI. The χ^2 for each solution is listed, as well

Table VI

Phase shift combinations
that give good agreement with experimental data

Solution	δ_0	δ_1	δ_3	χ^2	%
δ_0^-	$-33.4^\circ \pm 2.3$	$-0.7^\circ \pm 5.7$	$-0.1^\circ \pm 3.4$	10.6	21
δ_1^-	$-0.6^\circ \pm 3.2$	$-34.2^\circ \pm 2.3$	$-2.2^\circ \pm 2.5$	6.5	59
δ_1^+	$4.3^\circ \pm 2.7$	$35.4^\circ \pm 2.9$	$3.7^\circ \pm 1.8$	11.9	17

as the percentage probability of obtaining a χ^2 that large or larger, had that solution been the true solution. The δ_0^- and δ_1^- solutions correspond to virtually pure $s_{\frac{1}{2}}$- and $p_{\frac{1}{2}}$-wave phase shifts, respectively, of -33°. Both solutions also agree with the forward peaking in the cross section, indicating a repulsive nuclear potential. For the δ_1^+ solution the rise in the determined cross section at 25° and 35° does not agree with the predicted drop. Still other equally probable solutions may exist but have

not been found. The ambiguity between δ_0^- and δ_1^- is considered in greater detail in the Discussion.

VII DISCUSSION

A. Total Cross Section

Knowledge of the K^+-meson-proton interaction has been extended to intermediate kinetic energies. Our results in Table V confirm the increase in K^+-meson-proton cross section found from the scattering of K^+ mesons on free protons in emulsion.[1] Our averaged cross section over the energy interval from 200 to 300 Mev is 15.6 ± 1.0 mb, which agrees within the statistical errors with 18.0 ± 3.5 mb obtained from emulsion events (for comparison, the cross section below 100 Mev is 13.5 ± 2.5 mb).[2] The threshold for π-meson production by K^+ mesons on protons is 225 Mev. Our total cross sections include the contribution from π-meson production, but no estimate of the magnitude could be made.

Recent data from 600 Mev to 2 Bev indicate that the total cross section rises to 19.6 ± 1.2 mb at 700 Mev and then gradually drops to 13.0 ± 1.0 mb at 2 Bev.[12]

The over-all behavior of the K^+-meson-proton cross section as a function of energy is not understood at present.

B. The Nature of the K^+-Meson Force

Of the three phase-shift combinations that were found to fit the angular distribution of the scattered K^+ mesons, only two, namely δ_0^- and δ_1^-, gave good agreement with the small-angle scattering. Although both solutions are about equally probable, it is important to note that both correspond to a repulsive K^+-meson-proton force. This evidence in favor

of the repulsive nuclear force is indeed the most direct and conclusive. Less convincing evidence has come in the past from the optical-model analyses of inelastic scattering of K^+ mesons from emulsion nuclei.[1]

C. The Differential-Scattering Cross Section

The δ_0^- δ_1^- ambiguity in the phase-shift fitting to the experimental data cannot be easily resolved. It would be difficult to detect the polarization of the recoil proton given by[13]

$$P(\theta)=\frac{\left|\frac{\alpha}{1-\cos\theta}+\sin\delta_1 e^{i\delta_1}\cos\theta+i\sin\delta_1 e^{i\delta_1}\sin\theta\right|^2-\left|\frac{\alpha}{1-\cos\theta}+\sin\delta_1 e^{i\delta_1}\cos\theta-i\sin\delta_1 e^{i\delta_1}\cos\theta\right|^2}{\left|\frac{\alpha}{1-\cos\theta}+\sin\delta_1 e^{i\delta_1}\cos\theta+i\sin\delta_1 e^{i\delta_1}\sin\theta\right|^2+\left|\frac{\alpha}{1-\cos\theta}+\sin\delta_1 e^{i\delta_1}\cos\theta-i\sin\delta_1 e^{i\delta_1}\cos\theta\right|^2}$$

$$=\frac{\frac{2\alpha\sin\theta}{1-\cos\theta}}{\left[\frac{\alpha}{\sin\delta_1(1-\cos\theta)}\right]^2+\frac{\alpha}{\sin\delta(1-\cos\theta)}\left[2\cos\theta+\cos\delta\right]+1} \qquad (25)$$

which has a maximum of only 0.07 in the direction normal to the scattering plane for protons recoiling at 70° (lab), if the δ_1^- were the true solution. It may be easier to resolve the ambiguity by measuring the differential cross section of K^+ mesons scattering from protons at lower energies. If the differential cross section is isotropic for all energies and if one assumes that K^+ mesons scatter in the S wave at very low energies, then the δ_0^- phase-shift combination must be the true solution. This follows from the argument that to change from pure S-wave scattering to pure $P_{\frac{1}{2}}$-wave scattering the cross section must be anisotropic in the energy interval where both S and P waves contribute to the scattering cross section.

D. Use of K-p Dispersion Relations

The form of the K-p dispersion relations [14] is

$$D_+(\omega) = \frac{1}{4\pi^2}\int_1^\infty \frac{k'\sigma_+(\omega')}{\omega'-\omega}\,d\omega' + \frac{1}{4\pi^2}\int_1^\infty \frac{k'\sigma_-(\omega')}{\omega'+\omega}\,d\omega'$$

$$+\frac{1}{4\pi^2}\int_{\omega_{\Lambda\pi}}^{\infty} \frac{4\pi A_-(\omega')}{\omega'+\omega}\,d\omega' + \frac{\beta_\Lambda X(\Lambda)}{\omega_\Lambda+\omega} + \frac{\beta_\Sigma X(\Sigma)}{\omega_\Sigma+\omega} + C \qquad (26)$$

where D^+ is the real part of the K^+-proton forward-scattering amplitude in units of K-meson Compton wave length; K' is the laboratory-system momentum in units of $m_K c$; ω' and ω are laboratory-system energies of the K meson in units of $m_K c^2$; $\sigma_+(\omega')$ and $\sigma_-(\omega')$ are the K^+-p and K^--p total cross sections, respectively, in units of K-meson Compton wave length, squared; A_- is the imaginary part of the K^--p forward-scattering amplitude in units of K-meson Compton wave length, and C is a constant.

The purpose of this section is to investigate the possibility of determining unambiguously β_Λ (β_Σ) and $X(\Lambda)$ [$X(\Sigma)$], which are the sign and magnitude of the residues at $\omega = m_\Lambda (m_\Sigma)$ respectively, where

$$\chi_{\Lambda,\Sigma} = \frac{q^2_{\Lambda,\Sigma}}{4\pi} \cdot \frac{\left[\beta_{\Lambda,\Sigma}(m_{\Lambda,\Sigma} + \beta_{\Lambda,\Sigma} m_p)^2 - \beta_{\Lambda,\Sigma} m_K^2\right]}{4 m_p m_\Lambda} \qquad (27)$$

The quantity β_Λ (β_Σ) is either +1 or -1, depending upon whether the parity of the $K^-\Lambda$ ($K^-\Sigma$) is even or odd.

We have $$\omega_\alpha = \frac{m_\alpha^2 - m_p^2 - m_K^2}{2 m_p} \qquad (28)$$

where m_α is the rest energy of the α system ($\omega_\Lambda = 0.129\ m_K$, $\omega_\Sigma = 0.313\ m_K$, and $\omega_{\Lambda\pi} = 0.498\ m_K$).

By transforming from ω to $-\omega$, an expression for $D_-(\omega)$ is obtained,

(29)

Of the various subtracted dispersion relations proposed, none is adequate at present for the experimental data now available. The following form, however, has several decisive advantages:

$$\omega_0 D_+(\omega) - \tfrac{1}{2}(\omega_0+\omega) D_+(\omega_0) - \tfrac{1}{2}(\omega_0-\omega) D_-(\omega_0)$$

$$= \frac{1}{4\pi^2}\int_{\prime}^{\infty}\left[\frac{\omega_0 k'\sigma_+(\omega')}{\omega'-\omega} - \frac{(\omega_0+\omega)k'\sigma_+(\omega')}{2(\omega'-\omega_0)} - \frac{(\omega_0-\omega)k'\sigma_+(\omega')}{2(\omega'+\omega_0)}\right]d\omega'$$

$$+ \frac{1}{4\pi^2}\int_{\prime}^{\infty}\left[\frac{\omega_0 k'\sigma_-(\omega')}{\omega'+\omega} - \frac{(\omega_0+\omega)k'\sigma_-(\omega')}{2(\omega'+\omega_0)} - \frac{(\omega_0-\omega)k'\sigma_-(\omega')}{2(\omega'-\omega_0)}\right]d\omega'$$

$$+ \frac{1}{4\pi^2}\int_{\omega_{\wedge\pi}}^{\prime}\left[\frac{\omega_0 4\pi A_-(\omega')}{\omega'+\omega} - \frac{(\omega_0+\omega)4\pi A_-(\omega')}{2(\omega'+\omega_0)} - \frac{(\omega_0-\omega)4\pi A_-(\omega')}{2(\omega'-\omega_0)}\right]d\omega'$$

$$+ p_\wedge X(\wedge)\left[\frac{\omega_0}{\omega_\wedge+\omega} - \frac{\omega_0+\omega}{2(\omega_\wedge+\omega)} - \frac{\omega_0-\omega}{2(\omega_\wedge-\omega)}\right]$$

$$+ p_\Sigma X(\Sigma)\left[\frac{\omega_0}{\omega_\Sigma+\omega} - \frac{\omega_0+\omega}{2(\omega_\Sigma+\omega)} - \frac{\omega_0-\omega}{2(\omega_\Sigma-\omega)}\right] \qquad (30)$$

If ω_0 be made equal to m_k, Igi's form is obtained.[15] The above form, however, has the advantages of Igi's in that the cross-section integrals converge rapidly and depend more on the K^+-p cross sections than on the K^--p cross sections. These cross-section integrals converge even if the cross sections go to a constant as ω goes to infinity. It has an additional advantage of using the real parts of the forward-scattering amplitudes at energies for which they are known from experiment, rather than at the rest energy. Lastly, the contribution from the unphysical region is decreased by displacing a singularity from its position at m_k to ω_0.

The K^+-p total cross sections that were used were the emulsion data

of Table I for energies below 200 Mev, the results of this experiment, and recent counter data for the higher energies.[12] A smooth curve was fitted to the data and the statistical error on the curve was estimated to be 10%.

The low-energy K^--p total cross sections that were used were from hydrogen bubble chamber data. Elastic scattering, charge exchange scattering, and absorption were taken into account.[16,17,18] Furthermore, the total cross section is known from counter data to be 52 ± 9 mb at $\omega = 2.08$.[19] From preliminary hydrogen bubble chamber results the total cross section at $\omega = 2.52$ is 60 ± 20 mb.[20] The total cross section was assumed to be geometrical for protons (45 mb) at $\omega=4$. The above results were plotted as a function of energy and a smooth curve was passed through the points. A statistical error of 15% was estimated on the above-mentioned fit.

It was also found the k_{-abs} was approximately constant and equal to 14.4 for 1.06. This was the value chosen for $4\pi A_-$ at $\omega=1$, and a smooth extrapolation to zero at $\omega = 0.498$ was made in much the same way as done by Igi.[15] The integrals were numerically calculated with the cutoff at $\omega = 4$. The results of the integration are listed in Table VII.

The quantity $D_+= (\omega)$ was obtained from

$$D_{\pm}(\omega) = \pm \frac{W}{m_p}\sqrt{\frac{d\sigma_{\pm}^{el}}{d\Omega}\Big|_{\theta=0} - \frac{k_l^2}{16\pi^2}(\sigma_{\pm}(\omega))^2} \qquad (31)$$

where W and k_b are the total energy and K- meson momentum in the center-of-mass frame. The sign of $D_{\pm}$ (ω) is plus or minus, depending upon whether the K^+-proton force is attractive or repulsive, respectively.

Table VII

Results of numerical integration for different values of ω

Integral	ω			
	1.00	1.17	1.285	1.46
$\int_{\omega'=1}^{4} \frac{k'\sigma_+(\omega')d\omega'}{\omega'+\omega}$	19.62 ± 2.0	18.8 ± 1.9	19.41 ± 1.9	--
$\int_{\omega'=1}^{4} \frac{k'\sigma_+(\omega')d\omega'}{\omega'-\omega}$	57.59 ± 5.8	64.0 ± 7.7	64.15 ± 8.6	64.25 ± 9.8
$\int_{\omega'=1}^{4} \frac{k'\sigma_-(\omega')d\omega'}{\omega'+\omega}$	57.4 ± 8.6	55.7 ± 8.4	54.0 ± 8.1	51.38 ± 7.7
$\int_{\omega'=1}^{4} \frac{k'\sigma_-(\omega')d\omega'}{\omega'-\omega}$	--	192.5 ± 41.5	178.5 ± 29.7	--
$\int_{\omega'=.498}^{1} \frac{4\pi A_- d\omega'}{\omega'+\omega}$	3.38	2.78	2.88	2.56
$\int_{\omega'=.498}^{1} \frac{4\pi A_- d\omega'}{\omega'-\omega}$	--	-17.83	-13.21	--

From the experiment being described, it has been seen that the K^+-p interaction is repulsive, thus making $D_+(\omega)$ negative. The nature of the K^--p force is still unknown, and this causes $D_-(\omega)$ to be uncertain in sign.

From the δ_o^- phase-shift combination, $\frac{d\sigma_+^{el}(1.46)}{d\Omega}\Big|_{\theta=0}$ is 1.21±0.16 mb/sterad. If one assumes, as has been done here, that for lower K^+-meson energies $\frac{d\sigma_+^{el}(\omega)}{d\Omega}$ is isotropic, then $\frac{d\sigma_+^{el}(\omega)}{d\Omega}$ simply becomes $\frac{\sigma_+^{el}(\omega)}{4\pi}$. Furthermore, $\sigma_+^{el}(\omega) = \sigma_+(\omega)$ for $\omega < 1.46$. Thus sufficient information is available for the determination of $D^+(\omega)$ for ω= 1.0, 1.17, 1.285, and 1.46.

The value of $D_-(\omega)$ is obtained from Eq. (31) in a similar way but only for $\omega = 1.17$ and $\omega = 1.285$. From bubble chamber data we have

$$\left.\frac{d\sigma_-^{el}(1.17)}{d\Omega}\right|_{\theta=0} = 5.2 \pm 1 \text{ mb/sterad},$$

while $\left.\frac{d\sigma_-^{el}(1.285)}{d\Omega}\right|_{\theta=0}$ is still not available.[21] The total K^--p cross sections for the two energies are $\sigma_-(1.17) = 91 \pm 9$ mb and $\sigma_-(1.285) = 86 \pm 7$ mb. The value obtained for $D_-(1.17)$ is of the order of 0.5 K-meson Compton wave length. It is hoped that $D_-(1.17)$ is small enough to not introduce a significant ambiguity into the dispersion relation. For the higher energy, $D_-(1.285)$ is on the order of zero if $\left.\frac{d\sigma_-^{el}(1.285)}{d\Omega}\right|_{\theta=0}$ is assumed to be not much larger than 8.2 mb/sterad. This is not an unreasonable assumption, since $\sigma_-^{el}(1.285) = 44 \pm 8$ mb. The results of the calculations of $D_\pm(\omega)$ are listed in Table VIII.

Table VIII

$D_\pm(\omega)$ (the real part of the forward scattering amplitude) for different ω's

$D_\pm(\omega)$	ω			
	1.00	1.17	1.285	1.46
$D_+(\omega)$	$-.125 \pm 0.14$	-1.24 ± 0.14	-1.23 ± 0.14	-1.20 ± 0.08
$D_-(\omega)$	--	± 0.5	0	--

Now $p_\Lambda X(\Lambda)$ and $p_\Sigma X(\Sigma)$ will be determined for several combinations of ω and ω_0. Table IX lists the results of calculations for X_1, X_2, X_3, and X_4 where X_1 is the left-hand side of Eq. (30) with the $D_-(\omega_0)$ term

dropped out; X_2 is the sum of the three integrals on the right-hand side of Eq. (30) with a cutoff at = 4 on the first two; X_3 and X_4 are the respective coefficients of p X( ) and p X( ) in Eq. (30).

Table IX

Calculated values of X_1, X_2, X_3, and X_4 for different combinations of and .

		X_1	X_2	X_3	X_4
1.46	1.285	0.135±0.22	0.048±0.2	-0.238	-0.222
1.46	1.17	0.221±0.21	0.15±0.2	-0.411	-0.393
1.00	1.285	-0.211±0.24	-0.29±0.2	0.454	0.411
1.00	1.17	-0.117±0.22	-0.25±0.2	0.283	0.260

The values of X for different K-hyperon parities are given in Table X.

Table X

X( ), X( ) for even and add (X), parities

p	X( )	p	X( )
+1	$0.95g^2/4$	+1	$0.96g^2/4$
-1	$0.05g^2/4$	-1	$0.04g^2/4$

It was next assumed that the relative parities of the K and K pairs are the same, i.e., p = p = p. From the numbers listed in

Tables IX and X the quantity $pg^2/4\pi$ was evaluated for $p = \pm 1$, and the results are listed in Table XI for the various choices of ω and ω_o.

Table XI

Calculated values for the coupling constant for different combinations of ω and ω_o for the possibility of either a scalar or pseudoscalar coupling

ω	ω_o	$pg^2/4\pi$	
		p=+1	p=-1
1.46	1.285	$-0.20 \pm 0.68-0.20D_-(1.285)$	$-4.15 \pm 14-4.2D_-(1.285)$
1.46	1.17	$-0.09 \pm 0.38-0.19D_-(1.17)$	$-1.9 \pm 8-4.0D_-(1.17)$
1.00	1.285	$+0.09 \pm 0.38-0.17D_-(1.285)$	$+1.7 \pm 7-3.2D_-(1.285)$
1.00	1.17	$+0.25 \pm 0.58-0.16D_-(1.17)$	$+4.7 \pm 12-3.4D_-(1.17)$

In evaluation of $pg^2/4\pi$, the K^--proton forward-scattering amplitude was carried to the very end, in order to show what effect it has on the coupling constants. We see that for an attractive K^--p potential, D_- is positive and a pseudoscalar coupling is favored; for a repulsive K^--p potential D_- is negative and a scalar coupling is favored. If D_- is assumed to be negligible, the results from the first two rows favor a pseudoscalar coupling, from the second two rows, a scalar coupling. The value of $pg^2/4\pi$ varies about zero, but the variation is well within the statistical error. It is thus impossible to determine whether the coupling is scalar or pseudoscalar, but if it were scalar, $pg^2/4\pi$ would be less than about 0.6; if pseudoscalar, less than about 10. These results indicate that even with the most recently available data it is difficult,

from subtracted dispersion relations, to arrive at unambiguous conclusions as to the nature of the K-meson-hyperon coupling.

ACKNOWLEDGMENTS

I wish to express my sincere appreciation to Dr. Leroy Kerth and Mr. Ralph Baender for their assistance in all phases of the experiment. The encouragement and help of Dr. Robert Birge, Dr. Marian Whitehead, and Dr. Robert Lanou at all times were of the greatest value. Mr. Michael Austin, Mr. Victor Cook, Mr. Robert Matsen, Mr. Gerald Schnurmacher, and Mr. Thomas Tonisson are thanked for their assistance during the actual running of the experiment. I am grateful for the help of Mr. Robert Fry, Mrs. Edith Goodwin, Mrs. Beverly Jerome, Mr. Layton Lynch, Mr. David Marsh, Mrs. Marilynn Mc Laren, Mr. Joseph Waldman, and Mr. Robert Young in scanning the enormous length of film. Mr. Jonathan Young, for his skillful programming and running of the IBM-701 computer, and Dr. Edward Lofgren and the operating crew of the Bevatron, for their efficient operation of the machine, deserve grateful recognition.

I also wish to thank Dr. Robert Karplus for valuable discussions on the application of dispersion relations.

This work was done under the auspices of the U. S. Atomic Energy Commission.

Appendix A

Calculation of the Total K^+-p Cross Section

The K^+-p cross section is first expressed in a more convenient form, starting with Eq. (6), which is

$$\left.\frac{\bar{S}}{S_2}\right|_f - \left.\frac{\bar{S}}{S_2}\right|_e = \exp\left\{-\int_{x_0}^{x_1}(\lambda_s(x)+\lambda_0(x))dx\right\} - \exp\left\{-\int_{x_0}^{x_1}(\lambda_s(x)+\lambda_0(x))dx\right\}_f \quad \text{(A 1)}$$

The effect due to scattering of K^+ mesons off protons can be separated out from the term on the right for "target full" by

$$\exp\left\{-\int_{x_0}^{x_1}(\lambda_s(x)+\lambda_0(x))dx\right\}_f = \left\{-\int_{x_0}^{x_1}(\lambda'_s(x)+\lambda_0(x))dx - \sigma n l\right\}_f \quad \text{(A 2)}$$

$$= \exp\{-\sigma n l\}\exp\left\{-\int_{x_0}^{x_1}(\lambda'_s(x)+\lambda_0(x)dx\right\}_f, \quad \text{(A 3)}$$

where $\lambda'_s(x)$ no longer contains the effect of the protons in the target, but that effect has been integrated to give $\sigma n l$,

where σ is the total K^+-p cross section,

n is the number of protons per cm^3 in the target,

l is the length of the target in centimeters.

Equation (A 3) may be rewritten as

$$\exp\{-\Lambda_f\} = \exp\{-\sigma n l\}\exp\{-\Lambda'_f\}, \quad \text{(A 4)}$$

where the Λ's represent the integrals.

If $\left.\frac{\bar{S}}{S_2}\right|_f - \left.\frac{\bar{S}}{S_2}\right|_e$ may be represented by Δ, Eq. (A 1) becomes

$$\Delta = \exp\{-\Lambda_e\} - \exp\{-\sigma n l\} \exp\{-\Lambda'_f\}. \qquad \text{(A 5)}$$

Solving for $\sigma n l$, we get

$$\sigma n l = (\Lambda_e - \Lambda_f) - \ln(1 - e^{\Lambda_e} \Delta). \qquad \text{(A 6)}$$

The integrals were calculated for each K^+-meson energy and the results listed in Table A.I:

Table A.I

Parameters for the determination of σ, the K^+-p total cross section

Energy (Mev)	Parameters					
	$\Delta \times 10^3$	$\Lambda_e \times 10^2$	$(\Lambda_f - \Lambda_e) \times 10^3$	$\sigma n l \times 10^3$	% correction	σ (mb)
175 ± 25	10.41 ± 0.86	14.9 ± 0.2	1.9 ± 0.2	10.1 ± 1.1	-2.9	16.3 ± 1.7
225 ± 25	9.29 ± 0.76	12.6 ± 0.2	1.0 ± 0.1	9.4 ± 0.8	+1.1	15.2 ± 1.3
275 ± 25	9.82 ± 0.95	11.0 ± 0.2	0.66 ± 0.09	10.1 ± 1.1	+3.0	16.3 ± 1.7

Appendix B

Ring Counter Data

In the following matrices are given the numbers of times that various ring-counter combinations counted for target full and for target empty. Forward- and backward-scattering events correspond, respectively, to counting and not counting by the range counter R.

Target full (eff S_2 = 547516)

Forward scattering								Backward scattering							
Counters	Counters							Counters	Counters						
	A	B	C	D	E	F	G		A	B	C	D	E	F	G
1	22	12	5	6	3	6	8	1	13	11	1	1	1	5	3
2	13	24	11	4	5	3	10	2	7	16	9	1	1	2	1
3	9	13	14	6	3	4	6	3	13	4	11	3	0	1	0
4	5	2	13	15	3	8	7	4	3	4	9	5	5	0	1
5	11	17	9	14	16	10	5	5	5	3	5	12	8	4	3
6	8	12	10	3	16	9	11	6	4	4	2	7	4	5	3
7	19	24	21	11	9	22	30	7	3	6	6	1	2	6	11
8	17	10	18	10	6	12	19	8	3	3	6	7	3	3	15
1,2	20	18	0	5	2	0	3	1,2	7	14	10	1	3	2	1
2,3	10	10	16	4	2	0	0	2,3	2	4	12	12	0	0	0
3,4	4	7	19	19	5	0	0	3,4	1	1	13	15	10	0	0
4,5	1	0	5	26	9	1	4	4,5	4	2	5	11	13	0	3
5,6	4	3	6	5	12	6	17	5,6	1	2	3	5	8	11	19
6,7	6	6	4	3	5	14	29	6,7	1	2	3	2	5	14	38
7,8	0	4	2	3	3	7	16	7,8	0	0	2	3	1	3	8

Counters	Counters						Counters	Counters					
	A,B	B,C	C,D	D,E	E,F	F,G		A,B	B,C	C,D	D,E	E,F	F,G
1	28	30	3	0	0	1	1	42	33	0	0	0	0
2	22	18	4	1	1	1	2	12	6	14	0	0	0
3	5	14	9	7	2	1	3	3	7	5	10	1	1
4	3	9	12	11	4	1	4	5	2	5	5	1	0
5	5	4	3	10	9	11	5	2	1	2	8	17	7
6	2	1	3	1	13	14	6	0	0	2	3	8	4
7	0	5	3	3	13	15	7	2	0	0	4	7	18
8	2	8	1	2	1	17	8	0	1	2	2	1	2
1,2	31	50	19	0	0	1	1,2	22	70	28	2	0	0
2,3	12	16	39	18	1	0	2,3	15	27	53	29	3	0
3,4	2	11	23	40	12	7	3,4	1	15	13	66	30	4
4,5	2	2	10	35	57	22	4,5	2	1	8	23	71	27
5,6	0	2	0	15	30	31	5,6	0	2	12	8	19	22
6,7	3	2	1	11	17	27	6,7	0	0	1	4	5	19
7,8	1	0	0	0	8	9	7,8	1	0	0	1	3	4

Target empty (eff S_2 = 258063)

Forward scattering							
Counters	Counters						
	A	B	C	D	E	F	G
1	1	4	4	4	4	3	5
2	3	0	2	2	2	1	4
3	2	4	6	0	3	1	1
4	2	2	1	3	0	4	1
5	2	1	0	3	4	3	2
6	6	2	3	0	3	1	0
7	4	14	10	3	2	1	4
8	2	3	14	5	4	2	4
1,2	1	2	2	1	0	0	0
2,3	1	1	1	2	0	0	0
3,4	1	1	0	2	2	0	3
4,5	2	3	0	1	4	0	1
5,6	1	3	0	1	0	2	5
6,7	3	1	3	0	1	0	7
7,8	1	1	3	1	2	1	1

Backward scattering							
Counters	Counters						
	A	B	C	D	E	F	G
1	4	1	2	0	0	0	1
2	3	0	0	0	0	0	2
3	2	2	0	0	0	0	0
4	0	0	2	0	5	1	1
5	2	1	2	2	1	0	1
6	2	0	0	1	1	0	0
7	0	4	2	1	2	1	2
8	0	1	0	1	3	0	2
1,2	0	0	3	0	0	0	0
2,3	3	0	1	6	0	0	0
3,4	1	1	1	2	3	0	0
4,5	0	1	2	0	4	1	2
5,6	1	0	1	0	0	0	8
6,7	1	1	1	0	1	0	7
7,8	0	2	0	0	0	1	1

Counters	Counters					
	A,B	B,C	C,D	D,E	E,F	F,G
1	7	9	1	0	0	3
2	3	1	2	0	0	1
3	3	1	1	1	0	0
4	2	0	0	0	1	3
5	3	1	1	1	4	5
6	0	0	0	2	1	1
7	1	1	1	2	2	1
8	1	1	3	0	1	0
1,2	5	14	7	0	0	0
2,3	1	1	4	4	1	0
3,4	1	1	3	1	5	2
4,5	2	1	1	0	12	16
5,6	1	1	0	1	3	14
6,7	0	1	0	0	0	3
7,8	0	0	0	2	0	0

Counters	Counters					
	A,B	B,C	C,D	D,E	E,F	F,G
1	8	19	0	0	0	0
2	0	1	4	0	0	0
3	1	2	1	3	1	0
4	1	0	0	0	0	1
5	1	1	1	0	2	2
6	0	0	0	1	0	0
7	0	0	0	0	0	0
8	0	0	1	0	0	1
1,2	4	29	8	1	0	0
2,3	4	1	18	14	2	0
3,4	0	3	2	13	11	1
4,5	1	0	0	1	19	7
5,6	0	0	1	0	1	15
6,7	0	0	1	0	0	1
7,8	1	0	0	0	0	0

Appendix C

Determination of the Theoretical Decay Distribution

For this distribution only the charged decay products that entered a forward cone of half angle 50° with $\beta > 0.8$ were considered. This limiting value did not affect the predicted angular distribution to any extent since the cutoff affected only the rare decay modes. It could be seen in Fig. 11 that the $K_{\pi 2}$ and $K_{\mu 2}$ decay modes had $\beta > 0.8$ for forward decays. The angular distributions corresponding to these decay modes are shown in Fig. C1. To obtain these distributions it was necessary to assume only an isotropic decay distribution in the rest frame of the K^+ meson. The same assumption was made for the following decay modes.

The laboratory-system angular distribution of the positron from K_{e3} decay is shown in Fig. C . It was not necessary to know the energy distribution of the positron in the center-of-mass system but only to assume that its velocity was c, which indeed was a good assumption.

To obtain the distribution of the π^+ from $K_{\tau'}$ decay it was necessary to assume the energy distribution obtained from phase-space considerations alone.[22] Only 48% of the π^+ mesons were found to be sent forward and to have $\beta > 0.8$. The distribution of these energetic π^+ mesons is also shown in Fig. C2.

For the $K_{\mu 3}$ decay mode the energy distribution (center-of-mass system) was taken to be equal to the energy distribution of the 19 known events.[23] It was found that 72% of the decay events had a sufficiently high β, and their angular distribution is shown in Fig. C2.

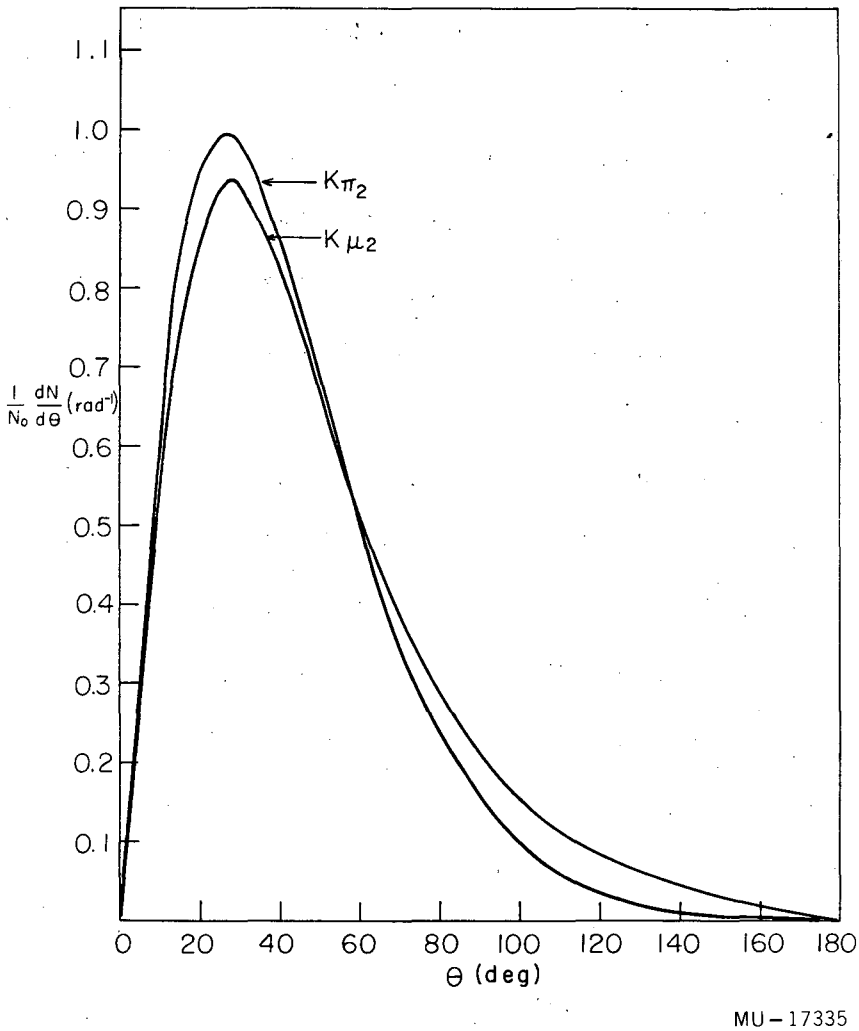

Fig. C 1. Angular distributions of the π^+ meson and μ^+ meson from $K\pi_2$ and $K\mu_2$ decays corresponding to a kinetic energy (lab) of 225 ± 25 Mev.

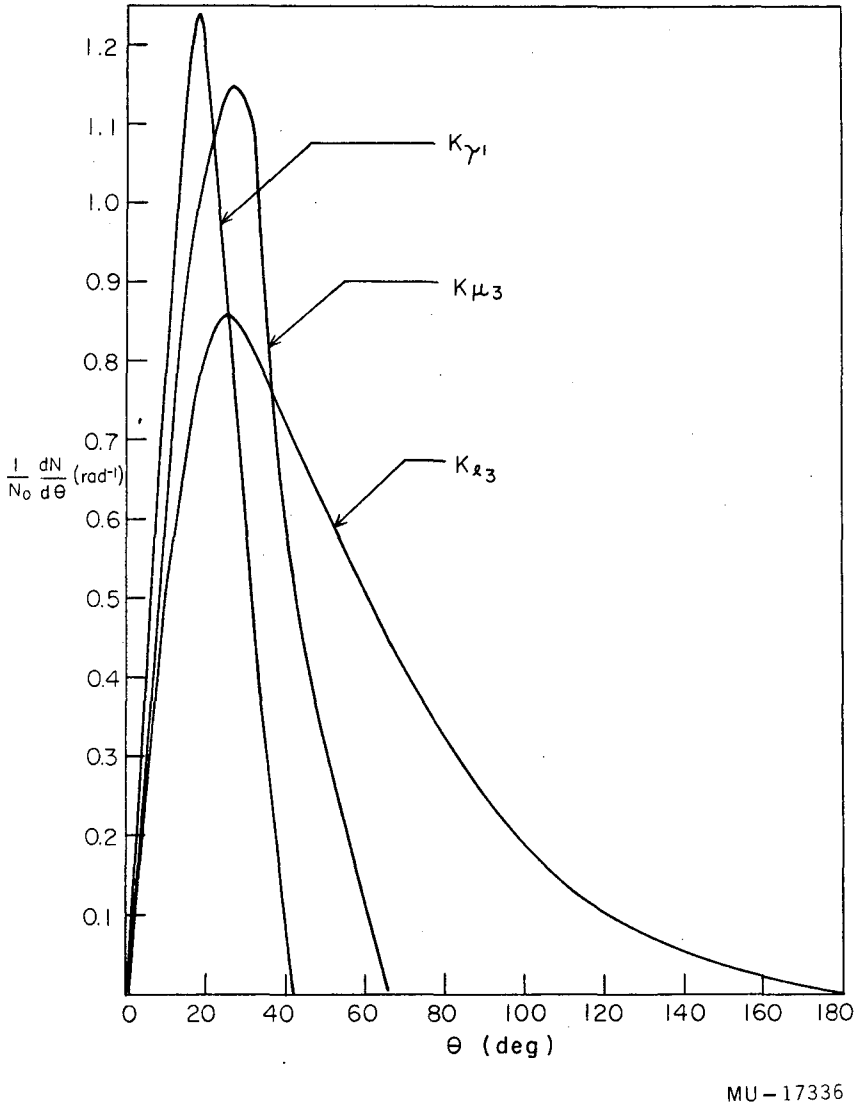

Fig. C 2. Angular distribution of the charged particle having $\beta > 0.8$ for the $K_{\tau'}$, K_{μ_3}, and K_{e_3} decay modes.

It was explained in the section on the water Cherenkov counter that for the K_{γ} decays, several factors enter in an prevent simulation of an event by a single charged π meson.

The weighted average of the five angular distributions shown in Figs. C1 and C2 is given in Fig. C3. The contribution to this predicted angular distribution from the three-body decay modes was less than 10% for all angles.

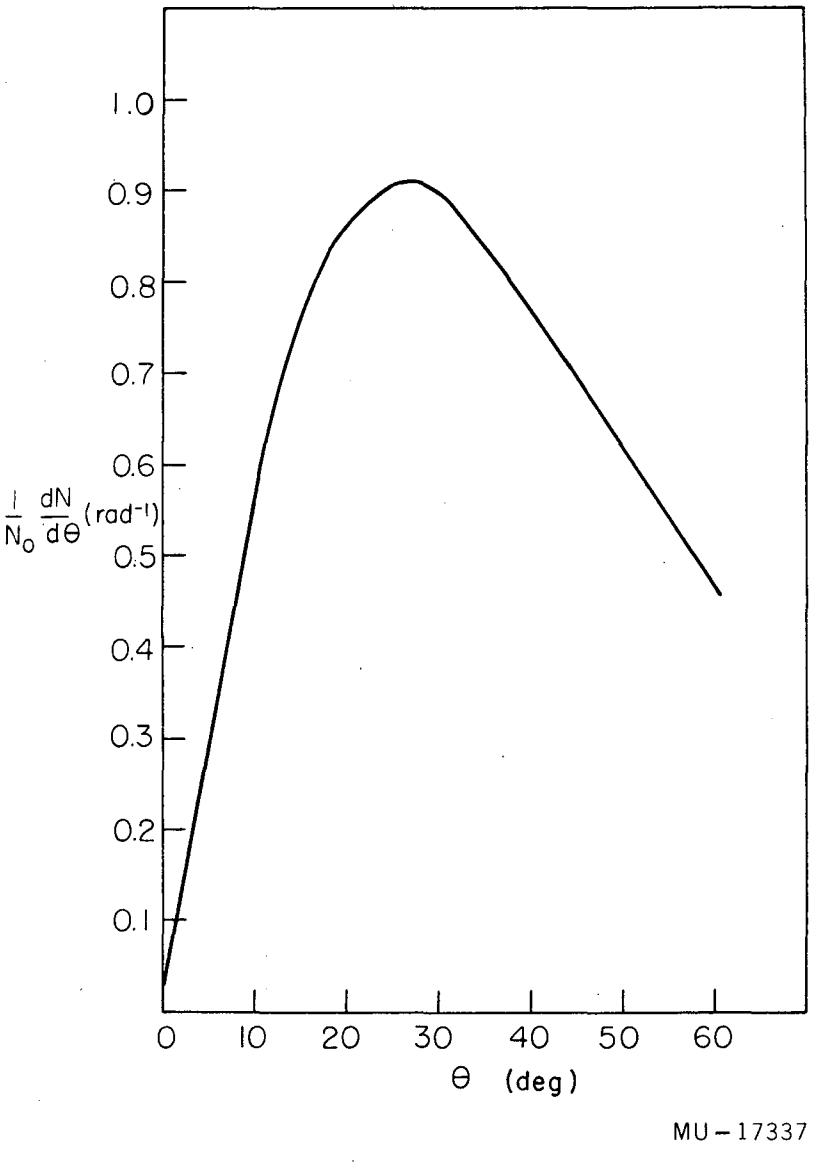

Fig. C 3. Composite weighted decay distribution of charged secondaries having $\beta > 0.8$ from K^+-meson decays.

Appendix D

Phase-Shift Fitting to the $\frac{1}{\lambda}\frac{d\sigma}{d\Omega}$ Data

The IBM 650 computer was programmed to fit $\frac{1}{\lambda^2}\frac{d\sigma(\mu)}{d\Omega}$, given in Eq. (23), to the differential-scattering cross-section points shown in Fig. 17. From a combination of the three phase shifts δ_0, δ_1, and δ_3, $\frac{1}{\lambda^2}\frac{d\sigma(\mu)}{d\Omega}$ was calculated and the χ^2 was obtained from Eq. (24). The angles were altered in steps which varied from 0.01 to 0.002 radian until χ^2 became a minimum. In order for the differential cross section at the minimum in χ^2 to be considered as a possible fit to the experimental data, only those were considered for which χ^2 is less than 14.7. This value corresponds to a 10% confidence level. By these criteria three possible solutions have been found and are listed in Table VI.

Next, the maximum deviation in each phase shift δ was obtained by varying the other two δ's for χ^2 fixed at 14.7. This deviation is a measure of the relative sensitivity of that phase shift to the fit, and is also given in Table VI.

REFERENCES

1. M. F. Kaplon, 1958 Annual International Conference on High Energy Physics at CERN.
2. D. H. Stork and D. J. Prowse (University of California, Los Angeles) private communication.
3. W. A. Wenzel, Millimicrosecond Coincidence Circuit for High-Speed Counting, UCRL-8000, October, 1957.
4. Alvarez, Crawford, Good, and Stevenson, in Proceedings of the Sixth Annual Rochester Conference on High Energy Physics, (Interscience Publishing Co., New York, 1957), Chap. VIII p. 29.
5. E. Helmy, J. H. Mulvey, D. J. Prowse, and D. H. Stork, An Example of the Production of a π^- Meson by a K^+ Meson (preprint).
6. Birge, Perkins, Peterson, Stork, and Whitehead, Nuovo cimento 4, 834 (1956).
7. E. Heiberg and J. Marshall, Rev. Sci. Instr., 27, 618 (1956).
8. G. Schnurmacher, A Diffuse-Reflection Coating for Use with Cherenkov Counters, UCID-691, March, 1959.
9. J. H. Atkinson, Jr. and B. H. Willis, High-Energy Particle Data, Vol. II, UCRL-2426 (Rev.), June, 1957.
10. W. A. Aron, The Passage of Charged Particles Through Matter (Thesis), UCRL-1325, May, 1951.
11. L. Van Hove, Phys. Rev. 91, 947 (1953).
12. Burrowes, Caldwell, Frisch, Hill, Ritson, and Schluter, Phys. Rev. Letters 2, 117 (1959).

13. E. Fermi, Phys. Rev. 91, 947 (1953).

14. A great deal has been written on the subject, but a few pertinent references are:

D. Amati and B. Vitale, Nuovo cimento 7, 190 (1958);

K. Igi, Progr. Theoret. Phys. (Kyoto) 3, 238 (1958);

C. Goebel, Phys. Rev. 110, 572 (1958);

P. T. Matthews and A. Salam, Phys. Rev. 110, 565 and 569 (1958).

15. K. Igi, Progr. Theoret. Phys. (Kyoto) 4, 403 (1958).

16. Nordin, Rosenfeld, Solmitz, Tripp, and Watson, Bull. Am. Phys. Soc. Ser. II, 4, 288 (1959).

17. Eberhard, Rosenfeld, Solmitz, Tripp, and Watson, Phys. Rev. Letters 2, 312 (1959).

18. A. H. Rosenfeld, Bull. Am. Phys. Soc. Ser. II 3, 363 (1958).

19. Cork, Lambertson, Piccioni, and Wenzel, Phys. Rev. 106, 167, (1957).

20. Alvarez, Eberhard, Good, Graziano, Ticho, and Wojcicki (Lawrence Radiation Laboratory) private communication.

21. Robert D. Tripp (Lawrence Radiation Laboratory) private communication.

22. R. H. Dalitz, Nuclear Phys. 1, 372 (1956).

23. J. Crussard, in Proceedings of the Sixth Annual Rochester Conference on High-Energy Physics (Interscience Publishing Co., New York, 1956), Chap. V p. 18.